Ni-Zn Hydroxide based bi-Phase Multiscale Porous Nanohybrids:

Physico-Chemical Properties

N. Habib[1,2], O. Guellati[1,2,3,*], A. Harat[1], A. Nait-Merzoug[1,2], J. El Haskouri[5], D. Momodu[4], N. Manyala[4], D. Begin[3] and M. Guerioune[1]

[1] *Laboratoire d'Etude et de Recherche des Etats Condensés (LEREC), Département de Physique, Université Badji-Mokhtar de Annaba, BP. 12, 23000 Annaba, ALGERIA.*

[2] *Université Mohamed Cherif Messadia de Souk Ahras, Fac. Sci, BP. 1553, 41000-Souk-Ahras, ALGERIA.*

[3] *Institut de Chimie et Procédés pour l'Energie, l'Environnement et la Santé (ICPEES) - ECPM - CNRS - UdS, 25 rue Becquerel, 67087 Strasbourg Cedex 2, FRANCE.*

[4] *Department of Physics, Institute of Applied Materials, SARCHI Chair in Carbon Technology and Materials, University of Pretoria, Pretoria 0028, SOUTH AFRICA.*

[5] *Instituto de Ciencias de los Materiales de la Universitat de València. C/ Catedrático José Beltrán, 2. 46980 Paterna, Valencia, SPAIN.*

****CorrespondingAuthor:** guellati23@yahoo.fr, tel : 00213670261228

Graphical Abstract
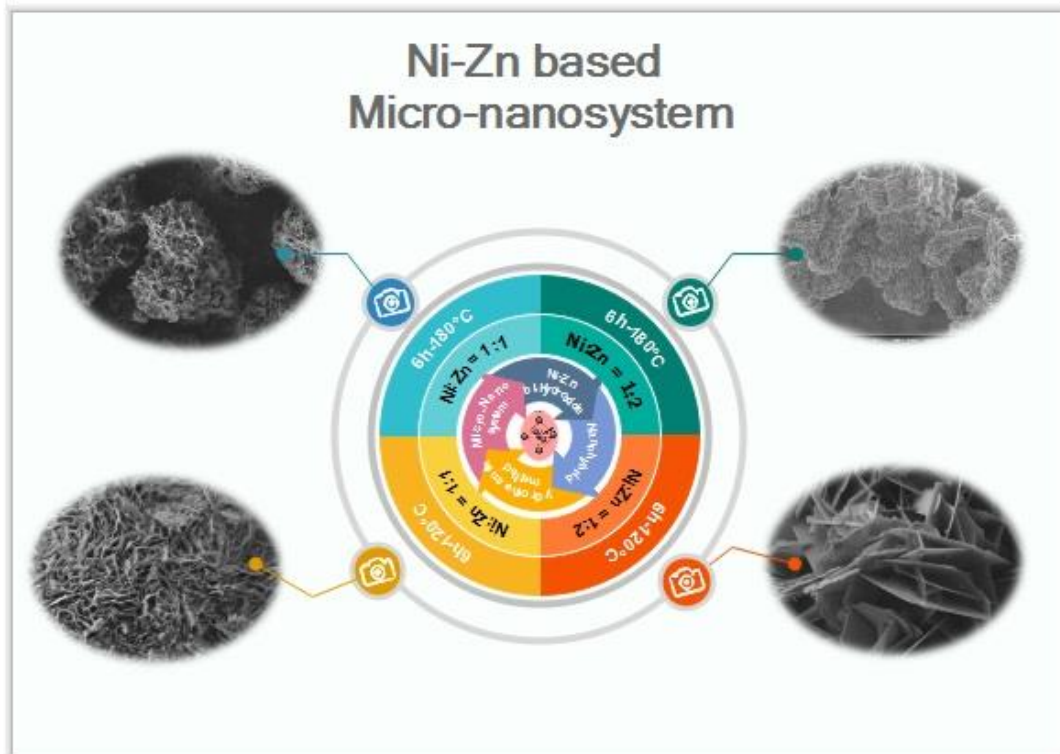
Highlights

1. Investigation of Hydrothermal Process Parameters: Effect on the Synthesized Ni/Zn Heterostructure Nanohybrid Morphology and Porosity.

2. Ni/Zn Precursors Ratio Effect on Bi-Phase Nanocomposites Synthesis for Ulterior Environnemental and Energy Application.

3. Physico-chemical Properties of Assembled Ni hydroxides and Zn Carbonate Hydroxides based Synthesised Heterostructure Nanohybrids.

Abstract

In this investigation, we report the synthesis of novel homogeneous micro–mesoporous bi-phase nanohybrids based on Ni/Zn hydroxides using a simple and low-cost free-template urea-based hydrothermal process at two different growth temperatures (120 and 180 °C) for 6 h in two cases of precursor ratios (Ni:Zn 1:1 and Ni:Zn 1:2). The synthesized products have been characterized with different techniques such as XRD, FT-IR, FESEM, Raman, BET and XPS analysis to identify quantitatively and qualitatively their original physico-chemical properties. The obtained structural results show the formation of bi-hydroxide-based products: -Ni(OH)2·0.75 H2O with Zn5(CO3)2(OH)6 (case Ni:Zn 1:1) or with Zn4(CO3)(OH)6·H2O (Ni:Zn 1:2) which are also proven by FTIR and Raman analyses. However, the obtained 3D micro–meso-nanohybrids with different pore morphology have been demonstrated through the FESEM micrographs depending on the synthesis conditions. Moreover, these porous products have been subjected to textural studies with the BET results showcasing a porous morphology with a reasonable specific surface area (SSA) and pore volume in the range (70–150 m2/g) and (0.19–0.85 cm3/g), respectively. Also, a clear improvement in the BET SSA (two times the initial value) was obtained with increasing the growth temperature in the two cases (1:1 and 1:2). Consequently, we have successfully synthesized active mesoporous materials with interesting specific surface area and porosity (pore volume and size) which make them attractive materials for electrode applications especially in energy storage and biosensing.

Keywords: micro-mesoporous materials, Layer double hydroxide, micro-nanohybrid, free-template hydrothermal synthesis, porosity.

Introduction

Nanoporous structured hydroxide based nanohybrids, precisely transition metal hydroxide based nanomaterials, have attracted much attention as a promising and active material choice in large scale applications such as: molecular adsorption/storage and separation for environment, ion exchange, nanotechnology, supercapacitor for energy storage and conversion, electro-biosensing, catalysts, etc (Bardé 2006 ; Li 2016; Gobal 2013); due to their unique properties which are strongly influenced by their composition, microstructure, **and** synthesis method (Mereu 2013; Choy 1998 ; Li 2015; Hu 2008).

These kind of nanomaterials possess high specific surface area, well-defined pore size distribution, and morphology as well **as** functional sites. Moreover, this porous materials can be classified as microporous (less than 2 nm), mesoporous (in the range of 2-50 nm) and macroporous (greater than 50 nm) with respect to their pore diameters (Gao 2014). In recent years, mesoporous materials has been the focus of scientists due to textural properties which are aligned with the application requirements from these diverse fields.

Numerous methods have been proposed for the synthesis of mesoporous nanostructures with controllable size, shape, and chemical stability such as hydrothermal process, sol-gel, chemical impregnation (Li 2015; Byrappa 2007 ; Lontio Fomekong 2015 ; Zhong 2005 ; Liu 2015). Moreover, the chemical and physical properties of these nanomaterial not only depend on their size, morphology and phase structure but also are influenced by their composition. Recent efforts have been focused on transition metal hydroxide nanocomposites with mixed metals taking into account their own properties. Among them, Nickel- and Zinc- based hydroxide nanomaterials have not been systematically studied for their large scale applications (Zheng 2017 ; Lai 2017; Jian 2017) as capacitor electrodes which are one of the oldest but still promising electrochemical energy storage solutions for hybrid/electric vehicules and portable electrical/electronic devices.

In this work, we report the successful synthesis of metallic (Ni or Zn) based carbonate $(CO_3)^{2-}$ and/or hydroxide $(OH)^-$ bi-structures in micro/nanoporous spheric nanohybrids using a simple one-step free-template urea based hydrothermal method, which is a high efficiency and low cost growth process. Furthermore, the present work is a novel report which provides a detailed and systematic approach to investigate the structural, morphological and electrochemical characteristics of NiZn based bi-transition metal hydroxides.

Experimental Procedure

All the chemicals, urea (Merck, purity $\geq$ 98%), Nickel and Zinc chloride (Sigma-Aldrich, purity $\geq$ 99.99%), were of analytical grade and were used without further purification.

1. Ni-Zn carbonate and/or hydroxide based heterostructure nanohybrids synthesis

0.1 M Nickel (II) chloride hexahydrate ($NiCl_2.6H_2O$) and 0.1 M Zinc (II) chloride ($ZnCl_2$) were dissolved in deionised water at room temperature (**25 °C**). After that, 0.5 M **Urea** (CH_4N_2O), which is highly soluble in water, was added into the above solution and ultrasonicated for 30 min until a dark green transparent solution was obtained which was transferred into a 40 mL Teflon-lined hydrothermal autoclave system. The autoclave was sealed, maintained at two different growth temperatures (120 and 180 °C) for 6 hours and then cooled down naturally to room temperature. The obtained products with different colors were filtered and washed with distilled water and ethanol several times, before drying in an oven at 80 °C overnight. Thereafter, a series of 3D crystalline heterometallic Ni-Zn hydroxide nanohybrids were synthesized using a free template hydrothermal process by changing the Ni/Zn precursors ratio (1:1 and 1:2) and growth temperature with keeping the same experimental conditions. The corresponding samples were designated as Ni- xZn -y °C (where x= 1 or 2; y = temperature growth).

2. Characterization techniques

The synthesized bi-phase nanohybrids were systhematically characterized by several analytical methods in order to study the effect of the hydrothermal process parameters on the products structural, morphology, and composition which have an influence on their electrochemical performance.

The structural characterization of Ni-Zn carbonate and/or hydroxide based nanohybrids were investigated by powder X-ray diffraction (XRD) using a XRD D8 ADVANCE-BRUKER AXS diffractometer, equipped with a copper anticathode tube ($\lambda_{CuK\alpha}$ = 1.5406 Å) and a graphite monochromator rear blade, operating at 40 kV - 40 mA and employing a scanning rate of $0.2°s^{-1}$. The XRD patterns of all specimens were recorded in the 2θ range of 10 to 90°.

The nanohybrid morphology was obtained using a field emission scanning electron microscopy FESEM (JEOL 6700-FEG microscope) operated at 3 kV.

Raman scattering measurements were carried out at room temperature with a Horiba JobinYvon Lab-RAM Aramis confocal Raman spectrometer equipped with a cooled CCD camera and an automated XYZ table, at a laser excitation of 532 nm. Using a D2 filter, the laser power that reached the samples was estimated as 0.33 mW.

Fourier-Transform InfraRed (FTIR) spectra were recorded using a BrukerVertex 77v spectrometer in the 400 to 4000 cm^{-1} range with a 4 cm^{-1} resolution controlled with an Opus software analysis software.

The Brunauer–Emmett–Teller (BET) specific surface area (SSA) measurements and the porosity distribution of the as-synthesized products were carried out on a Tristar an ASap2420 sorptometer (Micromeritics), using N_2 as adsorbent at liquid nitrogen temperature, through N_2 adsorption/desorption isotherms and the Barrett–Joyner–Halenda (BJH) method, respectively. Before measurements, the samples were initially out-gassed under vacuum overnight at room temperature to prevent material transformation and also to remove any impurities and moisture from the surface.

Surface chemical binding energies of the as-prepared layer double hydroxide (LDH) based nanohybrids were performed using X-ray photoelectron Spectroscopy in an ESCA+ equipment by Omicron. The system is equiped with a dual X-ray source ($Mg_{K\alpha} = 1253.6$ eV for our analysis, $Al_{K\alpha} = 1486.6$ eV), an electrostatic hemi-spherical analyser and detector with 7 channel trons. Depth profiling was performed using the ion gun, imaging (lateral resolution of 60 microns) and sample pretreatment were done in the reaction chamber. Binding energies were standardized by assigning the value of the C_{1s} peak to 284.6 +/- 0.2 eV relative to the Fermi energy level. The fitting procedure and the asymmetric peak deconvolutions were made using the "XPS Peak Fit and Casa XPS" programs where a Shirley background has been used and the Lorentzian-Gaussian (L/G) ratio was fixed at 30 %. It is a reliable technique to study the chemical states of bonded Ni-Zn elements on the surfaces of our nanohybrids by measuring their binding energy.

Results and Discussion

1. Structural properties

In this investigation, we start with the purity and the phase structure identification of our products. Figure 1 shows the powder XRD diffractograms of our products obtained using two different precursors ratio and growth temperature with their Inorganic Crystal Structure Database (ICSD) reference cards. The most obtained characteristic sharp and symmetric peaks show a typical XRD pattern of combination of two different transition metal hydroxide structures inside the synthesized nanohybrids with more nanocristalline nature.

As a result, samples with equimolar Ni/Zn precursors (1:1 ratio shown in Fig. 1a), synthesized at 120 °C and 180 °C for a 6h period can be indexed to a typical Rhombohedral lattices of Nickel Hydroxide Hydrate (α*-Ni-HH) (α*-Ni(OH)$_2$.0.75H$_2$O) and Zinc Carbonate Hydroxide (Zn-CH) (Zn$_5$(CO$_3$)$_2$(OH)$_6$) depending to the references cards [JCPDS 038-0715] and [JCPDS 19-1458], respectively. The diffraction peaks at 11.11°, 21.99°, 33.50° and 60.18° correspond to the α*-Ni-HH (003), (006), (101) and (110), respectively (Huang 2015).

Figure. 1. XRD patterns of obtained Ni–Zn 1:1 (a) and 1:2 (b) bi-phase nanohybrids using urea-based hydrothermal process with different experimental parameters
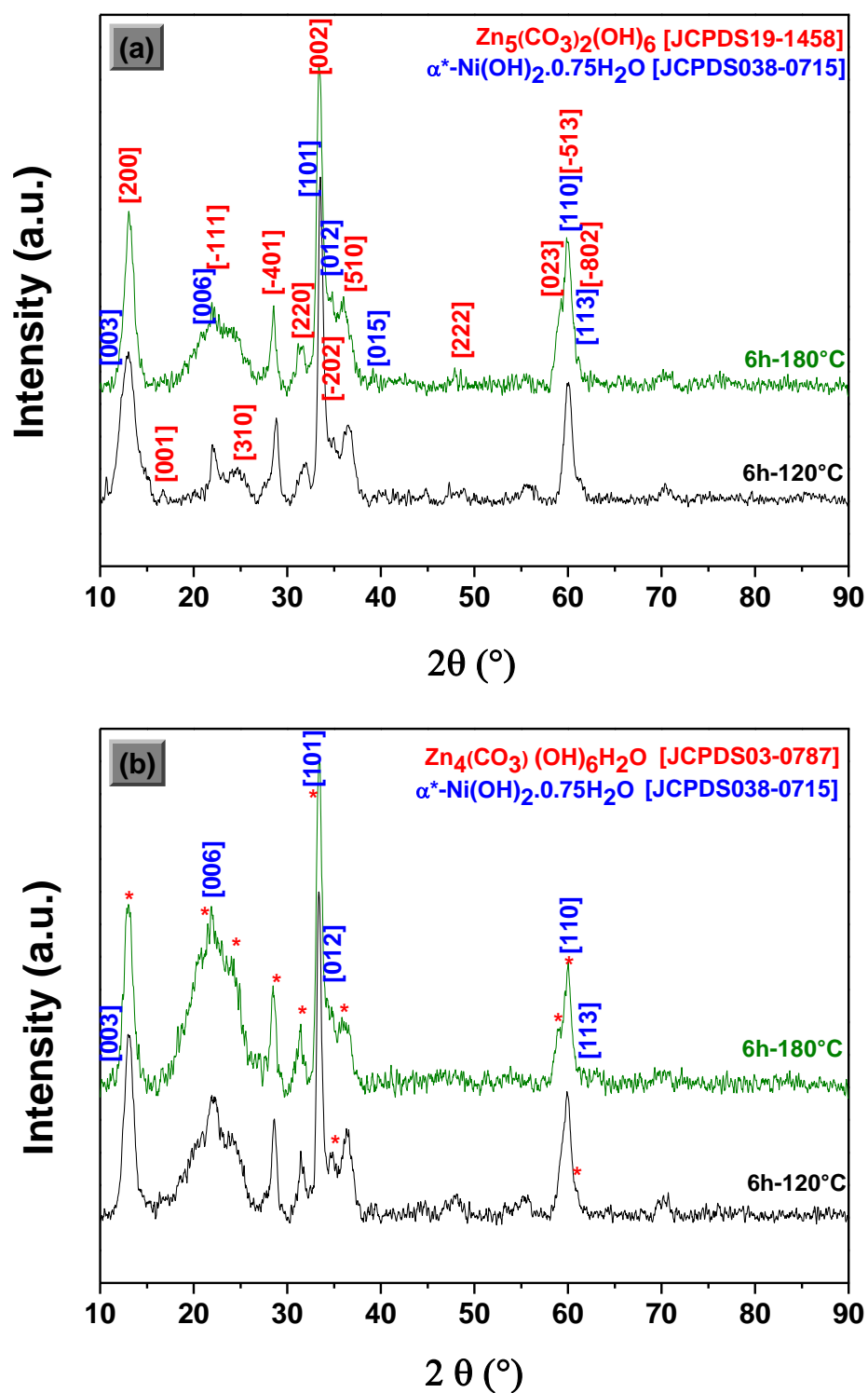
The existence of sharp peaks at 13.09°, 28.49°, 33.47° and 35.86° are attributed to the crystalline Zn-CH corresponding to (200), (020), (002) and (510) planes, respectively. This indexing clearly depicts a typical profile of layered hydroxide-based material (Choy 1998 ; Li 2015; Rojas 2008 ; Huang 2015) with the interlayer anions and their crystalline parameters as reported in Table 1, as well as the values of the $d_{(00l)}$ which determine the thickness of the brucite-like layer. From the first (003) peak position at a 2θ-value of approximately 11.11°, an interlayer distance of 7.77 Å could be estimated, which is in good agreement with those reported in the literature (7.79 Å for the spacing in α-Ni(OH)$_2$.0.75H$_2$O phase (Huang 2015)).

However, the XRD diffraction patterns of the second Ni/Zn precursors with a 1:2 ratio (Fig. 1b) correspond to the same α-Ni hydroxide (α-Ni-HH) phase but accompanied with another different Zn phase which is the Zinc Carbonate Hydroxide Hydrate (Zn-CHH) Zn$_4$(CO$_3$)(OH)$_6$.H$_2$O depending to the reference card [JCPDS 03-0787]. These patterns are characterized by an intense peak at 12.92° and with some others weak diffraction peaks at 21.85° and 33.31° confirming the layered structure (Choy 1998).

Thus, from the XRD analysis, it is worthy to state that the sample with precursor ratio of 1:1 gave a bi-structure rich with carbonate in comparison to the sample with the Ni/Zn precursor ratio of 1:2 which contains more hydroxides (LDH type structure) depending on the peak intensities.

FTIR analysis was also carried out to clarify the existing chemical bonds (see Fig. 2). From the results obtained, there exists several vibration bands where the key bands resemble those exhibited by hydrotalcite-like phase with CO$_3^{2-}$ as the counter anion (**Buazar 2016**). An intense broad absorption band centered at 3450 cm^{-1} was observed for the sample synthesized at 180 °C with a precursor molar ratio of 1:2 and 3500 cm^{-1} for the same sample synthesized at 120 °C. This is attributed to the stretching vibrations of the hydroxyl groups (O-H vibration) found on the surface and at the interlayer water molecules; this is also observed in the LDH materials and is comparable with the OH stretching vibration in free water active at 3600 cm^{-1} (Rojas 2004 ; Xie 2015 ; Ashassi-Sorkhabi 2016). The broad band at 3141 cm^{-1} accompanied by nearby band at 3023 cm^{-1} can be assigned to the hydrogen bonding between water and carbonate in the LDH interlayer. The band at 1605 cm^{-1} is assigned

Figure. 2. FTIR spectra of obtained Ni–Zn bi-phase nanohybrids using urea-based hydrothermal method with different experimental parameters
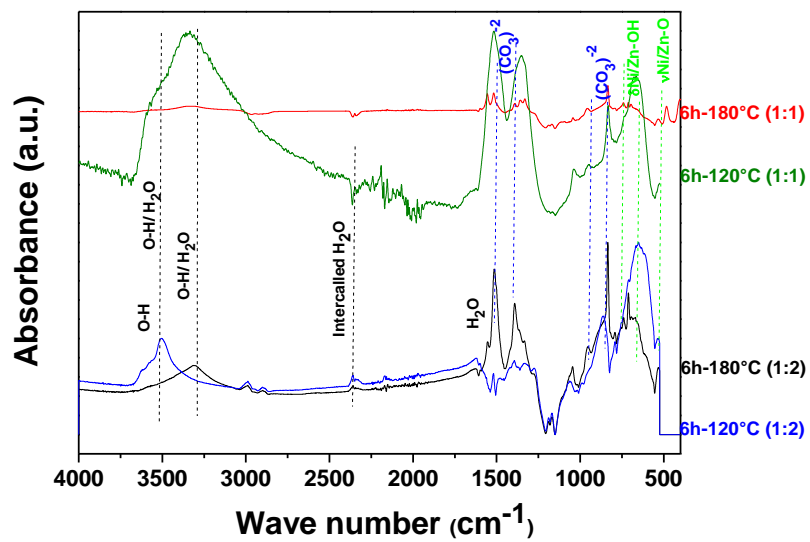
to the bending vibration of water molecules (Rojas 2004 ; Ashassi-Sorkhabi 2016 ; Ravi kumar 2017; Wang 2015).

In most of hydrotalcites, there are three IR active absorption bands arising from the carbonate anion observed at 1384 cm^{-1} (υ_3), 1058 cm^{-1} (υ_1) and 745 cm^{-1} (υ_2) (Ravi kumar 2017). The bands at 996 cm^{-1} and 826 cm^{-1} are associated with metal–oxygen (M–O) and metal–hydroxyl (M–OH) groups in the lattice of LDHs **(M can be Ni or Zn)** (Rojas 2004). Moreover, the sharp band at 835 cm^{-1} is associated with in-plane quadrant bending (Li 2015). Another peak at 1109 cm^{-1} is associated with C-O single bond stretching vibrations. In addition, below 646 cm^{-1}, the obtained bands are attributed to δNi/Zn-OH or ν Ni/Zn-O as reported in many studies (Wang 2015 ; **Buazar 2016 ; Koopi 2018**).

The Raman spectroscopy studies is shown in figure 3 to confirm the previous results. In detail, the spectra consisted of Raman-active bands at 106, 153, 392, 448, **(525-543)** and 737 cm^{-1}. The bands at 392, 448 and in the range **(525-543 cm^{-1})** indicate the presence of a Theophrastite Ni(OH)$_2$ phase depending to the reference (RRUFF ID: R070699) (Mohapatra 2017 ; Ramadoss 2016). Furthermore, the indexed peaks around 153 and 737 cm^{-1} show very good agreement with the reported values for Hydrozincite Zn$_5$(CO$_3$)$_2$(OH)$_2$ based nanomaterial depending on the reference (RRUFF ID: R050635). More precisely, the band located in the range **(525 – 543 cm^{-1})** can beassigned to the vibrations of the Ni–O/Zn–O symmetric stretching (A$_g$) mode (Mohapatra 2017).

However, the peak located at 448 cm^{-1} corresponds to a Ni–OH/Zn–OH symmetric (A$_{1g}$(T)) mode and an apparent band at 153 cm^{-1} is indicative of (E$_g$) symmetry mode (Mohapatra 2017).

Studies by Mohapatra's et al. (2017), indicate that Raman peaks observed at 106, 392, 448 and [525-543 cm^{-1}] could be linked to the E$_{2l}$, E$_{2h}$, E$_{2l}$, E$_{2h}$ and A$_l$(LO) multi-phonon modes**,** respectively. In general, a group theory

Figure. 3. Raman spectroscopy spectra of Ni–Zn (1:1 and 1:2)-based heterostructure hydroxides synthesized by hydrothermal method at two different growth temperatures
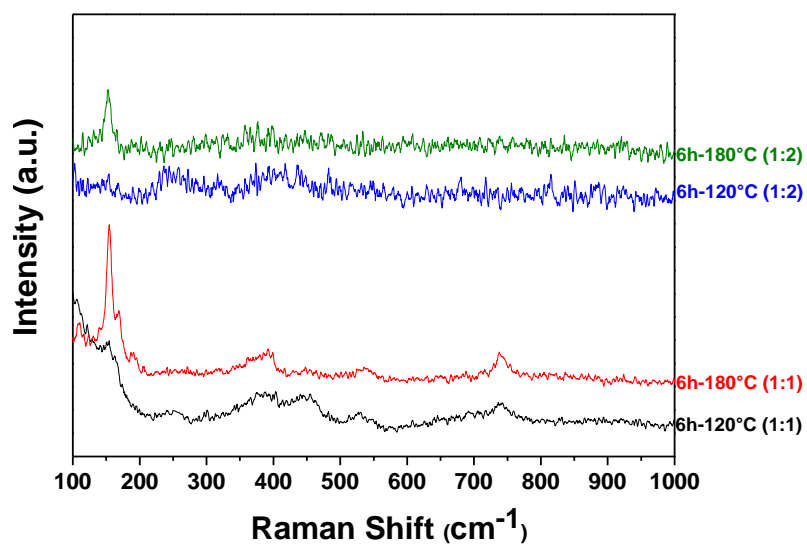
analysis of the phonon modes in brucite-type hydroxides predicts that four Raman active modes are found, three of which are lattices mode in the range (310-530 cm^{-1}) and one is a symmetric OH stretching vibration at around 3581 cm^{-1} (Mohapatra 2017 ; Ramadoss 2016 ; Oyedotun 2018). Thus, these results suggest also the formation of bi-phase nanohybrids based of Ni hydroxide and Zn carbonate hydroxide which is in agreement with the XRD and FTIR results.

2. Morphological and texturale properties

2.1. FESEM Results: Figure 4 shows the FESEM micrographs of these synthesized bi-phase nanohybrids with different quasi-microspherical framework (ranging from 6 to 25 μm) based on regular or irregular nanoflakes-like and sponge-shaped morphologies depending to the precursors ratio and growth temperature. The formation of very interesting 3D hierarchical micro/nanostructures with different kind of textural pores depending to the hydrothermal synthesis conditions is illustrated. The Ni-ions might have lowered the surface energy difference between the polar and nonpolar planes, leading to distinct morphologies (Kim 2017). However, with an increase in the amount of Zn-precursor into the Ni-solution in twofold (Fig. 4(c,d)), layered plate-like particles and individual spherical structures that were interconnected without clear boundaries formed continuous nanolayered structures, respectively. Notably, this kind of porous structure is favorable for efficient and fast ion transport to the surface of the active materials, which is interesting for the utilization of these active materials in specific conditions.

2.2. BET analysis Results: Figure 5 shows the N$_2$ adsorption/desorption isotherms and their corresponding BJH pore size distribution plots of the as-prepared bi-phase nanohybrids. It can be seen that these isotherms are typical Langmuir type IV characteristic according to IUPAC classification with an obvious hysteresis loop at a relative pressure (P/P$_0$) between 0.4–1.0, which indicates the existence of mesoporous structures (Wang 2015 ; Hu 2017).

The corresponding BET-SSA was determined to be in the range (52 – 127 m^2.g^{-1}) with an average pore size and volume in the range (12 – 32 nm) and (0.16 – 0.85 cm^3.g^{-1}), repectively, as reported in Table 1. In addition,

Figure. 4. FESEM micrographs of obtained micro-nanostructures based of Ni–Zn bi-phase nanohybrids at two different growth temperatures and Ni:Zn precursor ratios: 1:1 (a.a . 6 h–120 °C, b.b . 6 h–180 °C), 1:2 (c.c . 6 h–120 °C, d.d . 6 h–180 °C)
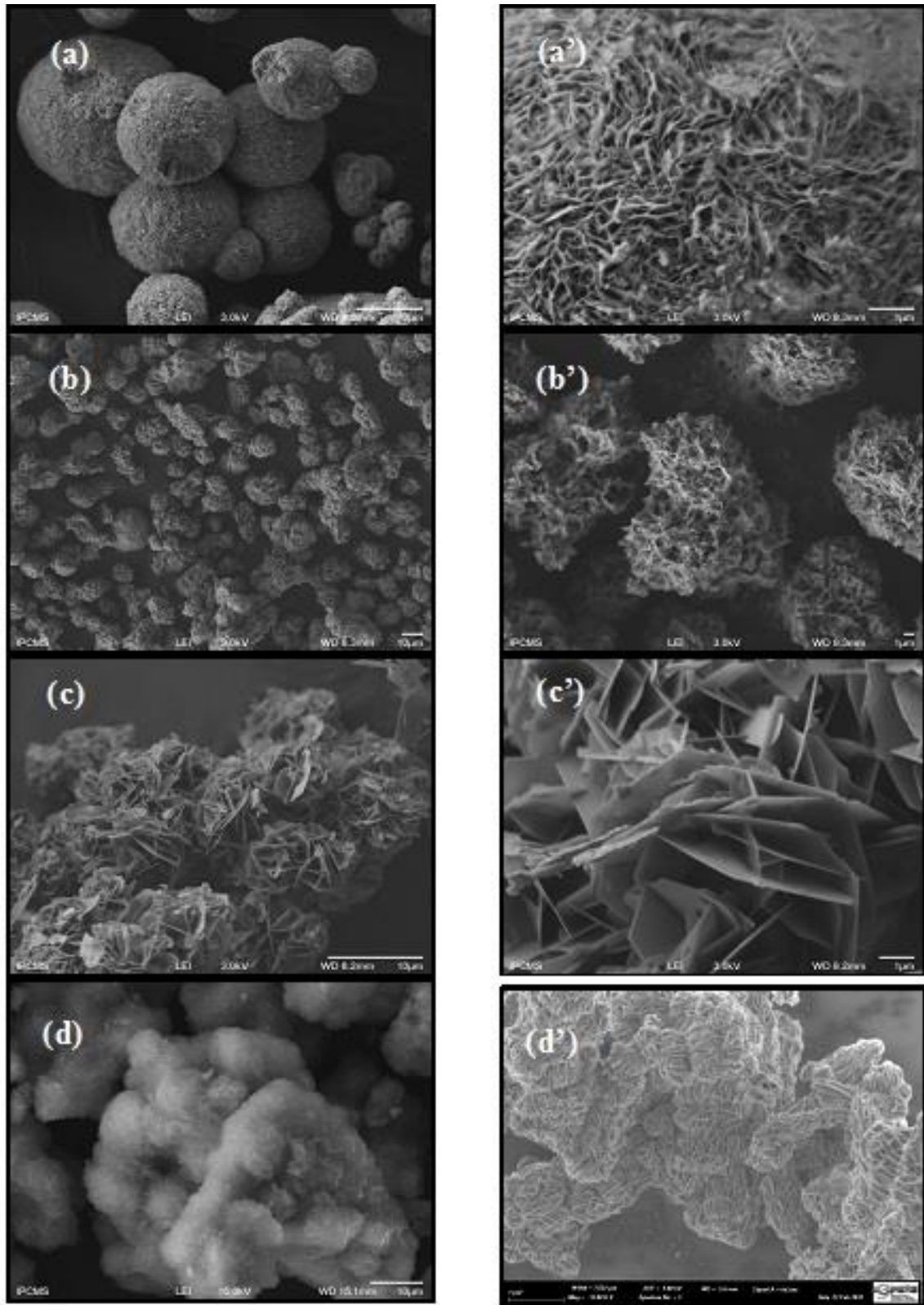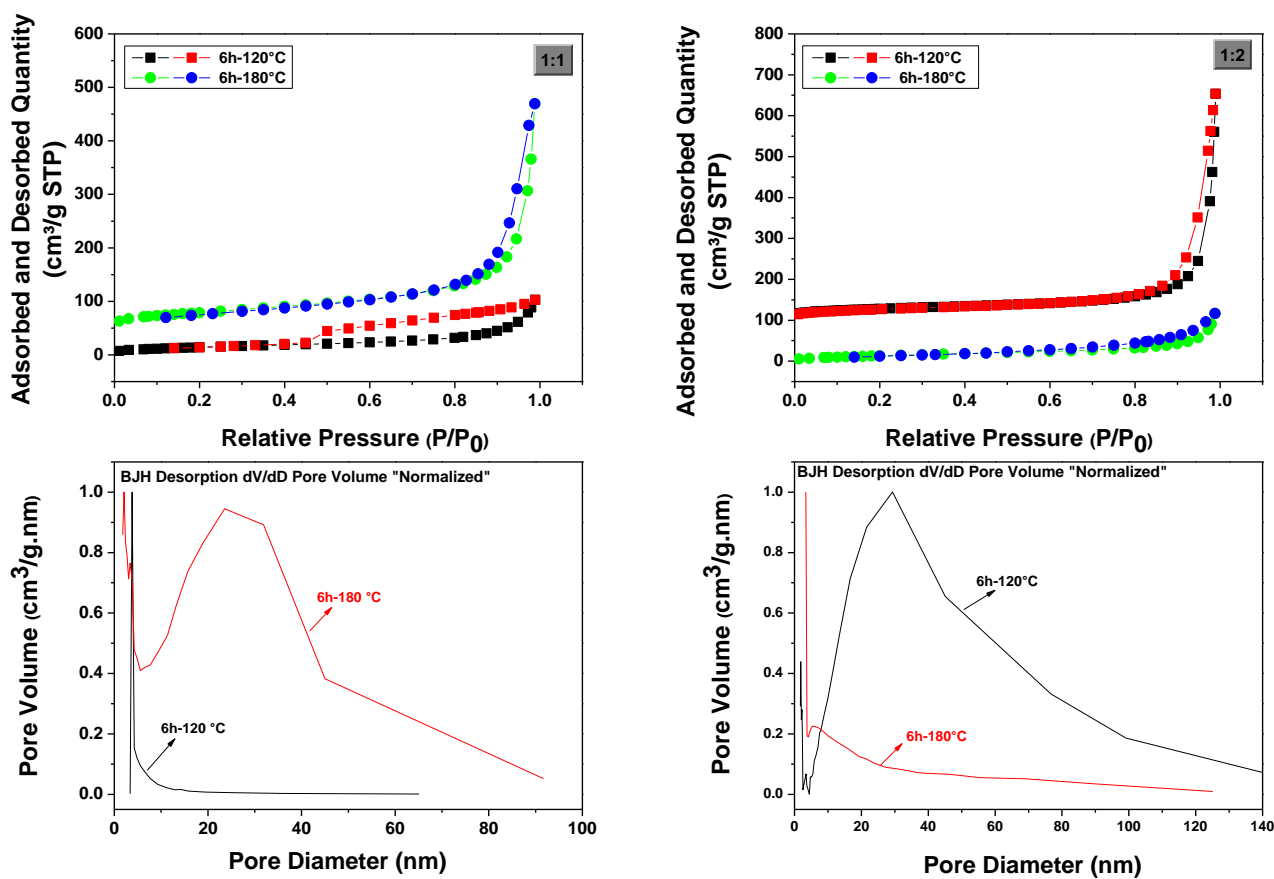
Figure. 5. N2 adsorption–desorption isotherms (up) and the corresponding pore size distribution (down) of the synthesized Ni–Zn-based micro-nanostructures using hydrothermal method at two different growth temperatures and Ni/Zn precursor ratios

with this quantitative analysis, we can clearly see the effect of the synthesis temparature. The SSA value increases to double the original value with increasing the hydrothermal synthesis temperature from 120 °C to 180 °C.

Table. 1: Physico-chemical characteristicsof the synthesized bi-hydroxide based 3D micro-nanohybrids.

bi-phase nanostructure		Crystalline parameters (Å)	BET-SSA (m^2/g)	BJH pore vol. (cm^3/g)	Pore diam. (nm)
1/1 α^*-Ni-HH+ Zn$_5$ CH	**(A)**	a = 3.10 Å, c = 24.11 Å a' = 13.85 Å, b' = 6.19 Å, c' = 5.48 Å, β = 101°	51.57	0.16	12.35
	(B)	a = 3.11 Å, c = 24.22 Å a' = 13.72 Å, b' = 6.24 Å, c' = 5.51 Å, β = 100.1°	126.70	0.66	20.81
1/2 α^*-Ni-HH+ Zn$_4$ CHH	**(C)**	a = 3.11 Å, c = 24.22 Å -	61.08	0.19	12.18
	(D)	a = 3.10 Å, c = 24.44 Å -	105.25	0.85	32.40

6h-120°C (A and C), 6h-180°C (B and D)

α^*-Ni-HH (**α^*-Ni(OH)$_2$.6H$_2$O**) (a = 3.08Å and c = 23.41 Å), Zn$_5$CH (**Zn$_5$(CO$_3$)$_2$(OH)$_2$**) (a' = 13.58 Å, b' = 6.28 Å, c' = 5.41 Å, β = 95.6°), Zn$_4$ CHH (**Zn$_4$(CO$_3$)(OH)$_6$.H$_2$O**) (crystalline parameters not found).

Therefore, these mesoporous nanostructures with a large surface area confirm their importance in a wide range of applications. More precisely, these nanoscale distributed pores would favor for example the fast diffusion of the electrolyte ions into these electroactive materials which will be used in our perspective investigation using these hydroxides as electroactive for supercapacitors.

3. XPS spectroscopy surface analysis results

In order to explore the surface elemental composition, the chemical valences and the oxidation states of bonded elements, the synthesized NiHH/ZnCH micro-nanosystems at different hydrothermal growth temperature and precursors ratio were also studiedand the corresponding binding energy (BE) values is shown in figure 6.

Figure. 6. XPS survey scan spectra (a) and percentage composition depending to the synthesis condition (b, c)
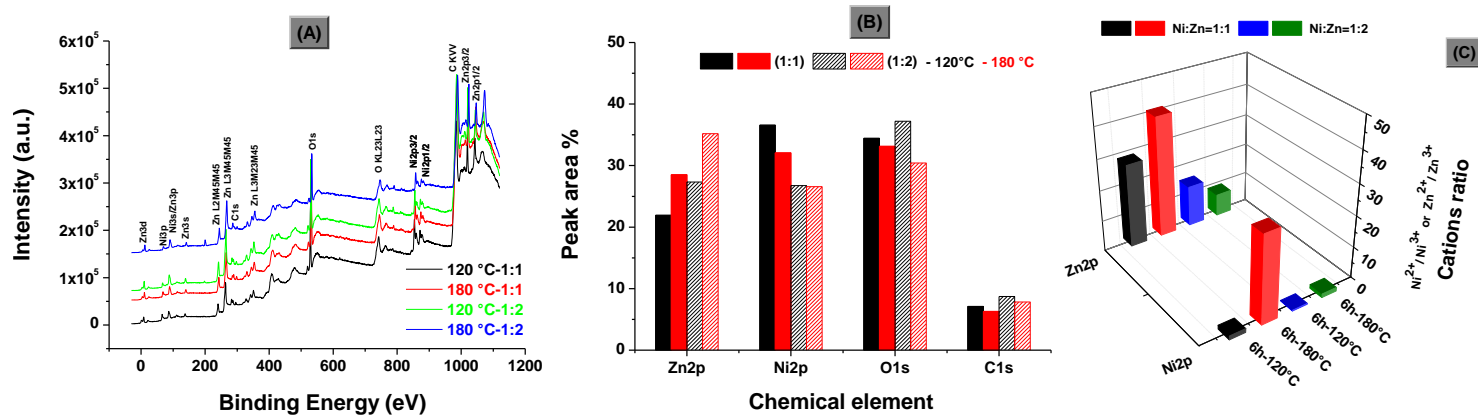
In figure 6A, the survey scan spectra for all the synthesized samples depicts the presence of Ni, Zn, C and O elements at their signatory binding energy position. Figure 6B displays the different percentage composition content of the deconvoluted parameters for the different synthesis conditions. In addition, we present the deconvolution of main spectra regions at high resolution core level spectra of the Ni_{2p}, Zn_{2p}, C_{1s}, and O_{1s} for all samples, using a L/G fitting method where the fitting parameters found on these spectra (binding energy, asymmetry of the main peak, intensity ratio between the main and the satellite peaks) are consistent with the literature data. Moreover, as reported in figure 6B, the area ratio of Zn_{2p} and Ni_{2p} in the products are around 0.6 - 0.89 and 1.2 - 1.5, respectively, for the Ni/Zn precursor ratios of 1:1 and 1:2 which agrees with the nanostuctures composition.

In the Ni_{2p} high resolution spectrum, not only two main peaks with binding energy around 854.1 - 857.6 eV and 861.6 - 867.3 eV associated with Ni^{2+} spin-orbit are found, but also peaks around 853.6 - 855.7 eV and 859.4 - 861.8 eV are fitted to be associated with Ni^{3+} spin-orbit indicating the presence of elemental Ni in the formation of $Ni(OH)_2$ hydroxide with some traces of metal Ni around 852.4 eV in some cases (Li 2015; Kim 2017; Hu 2017 ; Wang 2017). This high resolution scan also contains their two corresponding satellite peaks at around 873 eV and 879 eV with considerable intensities also found in many other related studies (Wang 2015 ; Kim 2017; Wang 2017; Fu 2016 ; Li 2017). These spin-orbit coupling with splitting energy gap of 17.6 ± 0.2 eV correspond to two major peaks $Ni_{2p3/2}$ and $Ni_{2p1/2}$, respectively, with two kinds of Ni species as reported by several works (Wang 2015 ; Ede 2017). Furthermore, we can clearly show that these Ni-Zn based hydroxides BE are shifted in compraison with values found in the literature with NiFe (Li 2015; Chen 2016), NiCo (Li 2015; Li 2017a; Chen 2016 ; Li 2017b), and NiAl (Li 2017a) hydroxide based nanocomposites.

Similarly, in the region of Zn_{2p} peaks, two spin-orbit doublets with their own adjacent obvious two apparent satellites (Sat.) were observed and the dominant fitted peaks centered around 1021 ± 1 eV and 1043 ± 1 eV could be ascribed to $Zn_{2p3/2}$ and $Zn_{2p1/2}$ (Zn-OH related binding states), respectively, of mostly Zn^{2+} oxidation state with a spin energy separation of 23 ± 0.1 eV (Wang 2015 ; Wang 2017; Mohamed 2017). We can found also some traces of Zn-OOH and O-deficient Zn^{1+} centered around 1023 eV and 1019 ± 1 eV, respectively, as reported in the work by Wang et al. (2017).

Consequently, Ni_{2p} and Zn_{2p} show that the oxidation state of these elements is the mixed state of two kinds of ions namely; Ni^{2+} (or Zn^{2+}) and Ni^{3+} (or Zn^{3+}), respectively, with different ratio as reported in figure 6C which agrees with those reported in other previous reports (Liang 2016).

In the case of the C_{1s} core level spectrum recorded, this was attributed to the samples containing the carbonate structural phase or signals picked up from the adhesive-carbon tape used as substrate during the XPS analysis. Different carbon-containing groups were obtained which include the C–C at 282.7 eV, C=C at 284.5 ± 0.3 eV (non oxygenated ring C), C–O (C–OH) at 286 eV (C in C–O bonds), C=O at 287 eV (carbonyl), O–CO around 288.2 ± 0.3 eV (carboxylate carbon) and (O-C=O) around 291 ± 1 eV (Li 2017). The predominant presence of the C=O, C–O and the O–H bonds confirm that the sample contains hydroxyl and carbonate groups with different percentage depending on the synthesis conditions.

In addition, the core level O_{1s} peaks found in these carbonate hydroxides are ascribed to the presence of a strong pronounced peaks centered around 529 ± 1 eV and 531 ± 0.3 eV illustrating the divalent state of O bonded as hydroxide (OH^-) groups (Li 2017).

It can also be bonded with metals to form metal oxides (O-M) and hydroxides (M-OH) (with M: Zn or Ni) (Wang 2015 ; Wang 2017; Li 2015).

The binding energy peak at 531.7 and 533.6 ± 0.1 eV appeared even more with second series of products (Ni:Zn = 1:2), which can be assigned to the contributions of adsorbed or crystal water (Li 2015). In particular, the recorded OH area was between 82 and 95 at.% of the total O_{1s} peak area which gives a balances between dominate (OH^-) hydrate and carbonate hydroxide (Wang 2017).

Consequently, these detailed reliable XPS analysis supports the previous results obtained from XRD and FTIR emphasizing the formation of pure Ni/Zn carbonate hydroxide nanohybrids with intercalated carbonate ions with different NiHH / ZnCH phases ratio and Ni^{2+}/Ni^{3+} (or Zn^{2+}/Zn^{3+}) ions ratio depending to the hydrothermal synthesis conditions. These results confirm that strong electron interactions occurred between Ni and Zn in this bi-hydroxide nanohybrid configuration.

Figure. 7. XPS spectra of these Ni–Zn bi-hydroxides micro-nanosystems in the Ni2p, Zn2p, C1s, and O1s energy regions at different conditions: (a: 6 h/120 °C and b: 6 h/180 °C)
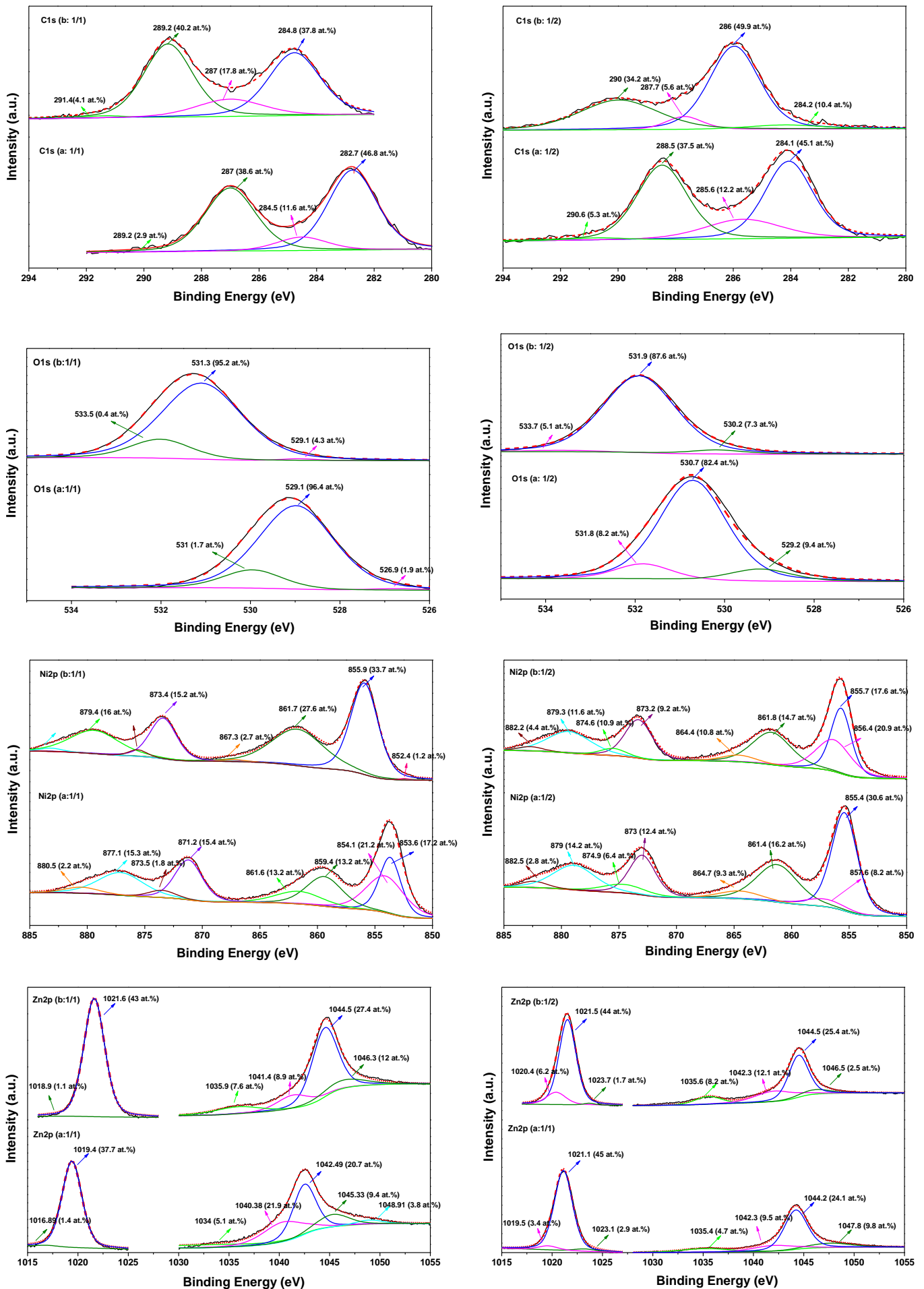
Conclusion

In this investigation, the intial part of the work reports on bi-structural Ni-Zn carbonate hydroxide based micro-nanohybrids synthesis using a simple and low cost hydrothermal process focusing mainly on the growth temperature and Ni/Zn precursors ratio effect on the structural, textural and morphological selectivity of the synthesized nanohybrids.

Therefore, the obtained results confirm the production of multiscale porous hydroxide based nanohybrids with regular or irregular nanoflakes-like and sponge-shaped morphologies in 3D hierarchical micro/ nanostructures with different kind of textural pores depending to the optimized hydrothermal synthesis conditions. The oxidation state in these products is the mixed state of two kinds of anions namely; Ni^{2+} (or Zn^{2+}) and Ni^{3+} (or Zn^{3+}), respectively, with different ratio depending to the growth conditions. These obtained morphological characteristics favorise the electrolyte ion diffusion, enhance the charge transport and provide more electroactive sites for fast electron/ion transfer energy storage.

These obtained mesoporous 3D architecture bi-hydroxide nanohybrids possessed very interesting specific surface area ($52 - 127$ $m^2.g^{-1}$) with reasonable pore volume ($0.16 - 0.85$ $cm^3.g^{-1}$) and pore size distribution ($12 - 32$ nm) which can provide additional active sites to facilitate the rapidions diffusion and penetration or electron/ ion transfer.

Consequently, these hierarchically nano-porous transition bi-metal hydroxides and carbonate hydroxides structures based of Ni and Zn should be promising electroactive materials in the fabrication of half-cell device electrodes for mostly energy storage, environment, and sensing applications in perspective.

References

Ashassi-Sorkhabi H, La'le Badakhshan P, Asghari E (2016) Electrodeposition of three dimensional-porous Ni/Ni(OH)$_2$ hierarchical nano composite via etching the Ni/Zn/Ni(OH)$_2$ precursor as a high performance pseudocapacitor. Chem. Eng. J. 299(1) : 282–291. http://dx.doi.org/10.1016/j.cej.2016.04.069

Bardé F, Palacín M.R, Beaudoin B, Christian P.A, Tarascon J.M (2006) Cationic substitution in γ-type nickel (oxi) hydroxides as a means to prevent self-discharge in Ni/Zn primary batteries. J. Power Sourc. 160 : 733–743. https://doi.org/10.1016/j.jpowsour.2005.12.073

Buazar F, Baghlani-Nejazd M.H, Badri M, Kashisaz M, Khaledi-Nasab A and Kroushaw F (2016) Facile one-pot phytosynthesis of magnetic nanoparticles using potato extract and their catalytic activity. Starch/Stärke 68 : 1–9. DOI: 10.1002/star.201500347

Buazar F, Bavi M, Kroushawi F, Halvani M, Khaledi Nasab A & Hossieni S.A (2015) Potato extract as reducing agent and stabiliser in a facile green one-step synthesis of ZnO nanoparticles. Journal of Experimental Nanoscience 11 (3) : 1-10. https://doi.org/10.1080/17458080.2015.1039610

Byrappa K, Adschiri T (2007) Hydrothermal technology for nanotechnology. Prog. Cryst. Growth Charact. Mater. 53 (2) : 117–166. https://doi.org/10.1016/j.pcrysgrow.2007.04.001

Chen J, Xu J, Zhou S, Zhao N, Wong C.P (2016) Amorphous nanostructured FeOOH and Co-Ni double hydroxides for high-performance aqueous asymmetric supercapacitors. Nano Energy 21 : 145–153. https://doi.org/10.1016/j.nanoen.2015.12.029

Choy J.H, Kwon Y.M, Han K.S, Song S.W, Chang S.H (1998) Intra- and inter-layer structures of layered hydroxy double salts, $Ni_{1-x}Zn_{2x}(OH)_2(CH_3CO_2)_{2x} \cdot nH_2O$. Mater. Lett. 34 : 356–363. PII S0167-577X 97 00191-2

Ede S.R, Anantharaj S, Kumaran K.T, Mishra S, Kundu S (2017) One step synthesis of $Ni/Ni(OH)_2$ nano sheets (NSs) and their application in asymmetric supercapacitors. RSC Adv. 7 : 5898–5911. DOI: 10.1039/C6RA26584G

Fu W, Wang Y, Han W, Zhang Z, Zha H, Xie E (2016) Construction of hierarchical $ZnCo_2O_4@Ni_xCo_{2x}(OH)_{6x}$ core/shell nanowire arrays for high-performance supercapacitors. J. Mater. Chem. A 4 : 173–182. DOI: 10.1039/C5TA07965A

Gao F, Li W.M, Hou Y.J (2014) Investigation for Mechanical Properties of Porous Materials Based on Homogenization Theory. Advanced Materials Research. Adv. Mater. Res. 1048 : 414–417. doi:10.4028/www.scientific.net/AMR.1048.414

Gobal F, Faraji M (2013) Fabrication of nanoporous nickel oxide by de-zincification of Zn – Ni /(TiO$_2$-nanotubes) for use in electrochemical supercapacitors. Electrochim. Acta. 100 : 133–139. DOI: 10.1016/j.electacta.2013.03.155

Hu B, Chen S.F, Liu S.J, Wu Q.S, Yao W.T, Yu S.H, (2008) Controllable synthesis of zinc-substituted α- and β-nickel hydroxide nanostructures and their collective intrinsic properties. Chem. - A Eur. J. 14 : 8928–8938. DOI: 10.1002/chem.200800458

Hu W, Wei H, She Y, Tang X, Zhou M, Zang Z, Du J, Gao C, Guo Y, Bao D (2017) Flower-like nickel-zinc-cobalt mixed metal oxide nanowire arrays for electrochemical capacitor applications. J. Alloys Compd. 708 (25) : 146-153. https://doi.org/10.1016/j.jallcom.2017.02.301

Huang J, Yang Z, Wang R, Zhang Z, Feng Z, Xie X (2015) Zn–Al layered double oxides as high-performance anode materials for zinc-based secondary battery. J. Mater. Chem. A 3 : 7429-7436. DOI: 10.1039/c5ta00279f

Jian Y, Wang D, Huang M, Jia H.L, Sun J, Song X, Guan M (2017) Facile Synthesis of Ni(OH)$_2$/Carbon Nanofiber Composites for Improving NiZn Battery Cycling Life. ACS Sustain. Chem. Eng. 5 : 6827–6834. DOI: 10.1021/acssuschemeng.7b01048

Kim D.Y, Ghodake G.S, Maile N.C, Kadam A.A, Sung Lee D, Fulari V.J, Shinde S.K (2017) Chemical synthesis of hierarchical NiCo$_2$S$_4$ nanosheets like nanostructure on flexible foil for a high performance supercapacitor. Sci. Rep. 7 : 9764–9773. doi: 10.1038/s41598-017-10218-z

Koopi H, Buazar F (2018) A novel one-pot biosynthesis of pure alpha aluminum oxide nanoparticles using the macroalgae Sargassum ilicifolium: A green marine approach, Ceramics International 44 (8) : 8940-8945. https://doi.org/10.1016/j.ceramint.2018.02.091

Lai S.B, Jamesh M.I, Wu X.C, Dong Y.L, Wang J.H, Gao M, Liu J.F, Sun X.M (2017) A promising energy storage system: rechargeable Ni–Zn battery. Rare Met. 36 : 381-396. DOI 10.1007/s12598-017-0905-x

Li D, Li Y, Zhao J, Xu Z, Zhang H (2017) Three-dimensional porous layered double hydroxides growing on carbon cloth as binder-free electrodes for supercapacitors. J. Mater. Res. 32 (13) : 2487–2496. https://doi.org/10.1557/jmr.2017.227

Li G.C, Liu P.F, Liu R, Liu M, Tao K, Zhu S.R, Wu M.K, Yi F.Y, Han L (2016) MOF-derived hierarchical double-shelled NiO/ZnO hollow spheres for high-performance supercapacitors. Dalt. Trans. 45 (34): 13311–13316. doi: 10.1039/c6dt01791f

Li H.B, Gao Y.Q, Yang G.W (2015) Electrochemical route for accessing amorphous mixed-metal hydroxide nanospheres and magnetism. RSC Adv. 5 : 45359-45367. DOI: 10.1039/c4ra14370a

Li J, Wei M, Chu W, Wang N (2017) High-stable A-phase NiCo double hydroxide microspheres via microwave synthesis for supercapacitor electrode materials. Chem. Eng. J. 316 (15) : 277–287. https://doi.org/10.1016/j.cej.2017.01.057

Liang D, Wu S, Liu J, Tian Z, Liang C (2016) Co-doped Ni hydroxide and oxide nanosheet networks: laser-assisted synthesis, effective doping, and ultrahigh pseudocapacitor performance. J. Mater. Chem. A 4 : 10609–10617. DOI:10.1039/C6TA03408J

Liu J, Wang J, Zhang X, Fang B, Hu P, Zhao X (2015) Preparation and structural characterization of switterionic surfactant intercalated into NiZn-layerd hydroxide salts. J. Phys. Chem. Solids 85 : 180–187. https://doi.org/10.1016/j.jpcs.2015.05.017

Lontio Fomekong R, Kenfack Tsobnang P, Magnin D, Hermans S, Delcorte A, Lambi Ngolui J (2015) Coprecipitation of nickel zinc malonata : A facile and reproducible synthesis route for $Ni_{1-x}Zn_xO$ particles and $Ni_{1-x}Zn_xO$/ZnO nanocomposites via pyrolysis. J. Solid State Chem. 230 : 381–389. https://doi.org/10.1016/j.jssc.2015.07.040

Mereu R.A, Mesaros A, Petrisor T, Gabor M, Popa M, Ciontea L, Petrisor T (2013) Synthesis, characterization and thermal decomposition study of zinc propionate as a precursor for ZnO nano-powders and thin films. J. Anal. Appl. Pyrolys. 104 : 653–659. DOI: 10.1016/j.jaap.2013.05.001

Mohamed S.G, Attia S.Y, Allam N.K (2017) One-step, calcination-free synthesis of zinc cobaltite nanospheres for high-performance supercapacitors. Mater. Today Energy 4 : 97–104. https://doi.org/10.1016/j.mtener.2017.04.003

Mohapatra D, Parida S, Badrayyana S, Singh B.K (2017) High performance flexible asymmetric CNO-ZnO//ZnO supercapacitor with an operating voltage of 1.8 V in aqueous medium. Appl. Mater. Today 7 : 212-221. https://doi.org/10.1016/j.apmt.2017.03.006

Oyedotun K.O, Madito M.J, Momodu D.Y, Mirghni A.A, Masikhwa T.M, Manyala N (2018) Synthesis of ternary $NiCo-MnO_2$ nanocomposite and its application as a novel high energy supercapattery device. Chem. Eng. J. 335 (1) : 416–433. https://doi.org/10.1016/j.cej.2017.10.169

Ramadoss A, Kang K.N, Ahn H.J, Kim S.I, Ryu S.T, Jang J.H (2016) Realization of high performance flexible wire supercapacitors based on 3-dimensional $NiCo_2O_4$/Ni fibers. J. Mater. Chem. A 4 : 4718–4727. DOI: 10.1039/C5TA10781D

Ravi kumar C.R, Kotteeswaran P, Raju V.B, Murugan A, Santosh M.S, Nagaswarupa H.P, Prashantha S.C, Kumar M.R.A, Shivakumar M.S (2017) Influence of zinc additive and pH on the electrochemical activities of β-nickel hydroxide materials and its applications in secondary batteries. J. Energy Storage 9 : 12–24. https://doi.org/10.1016/j.est.2016.11.001

Rojas R, Ángeles Ulibarri M, Barriga C, Rives V (2008) Intercalation of metal-edta complexes in Ni-Zn layered hydroxysalts and study of their thermal stability. Microporous Mesoporous Mater. 112 : 262–272. doi:10.1016/j.micromeso.2007.09.042

Rojas R, Barriga C, Ulibarri M.Á, Rives V (2004) Intercalation of vanadate in Ni, Zn layered hydroxyacetates. J. Solid State Chem. 177 : 3392–3401. doi:10.1016/j.jssc.2004.05.055

Wang S, Wang X, Bao Z, Yang X, Ye L, Zhao L (2017) An evenly distributed sulfur-doped nickel zinc hydroxyl carbonate dispersed structure for all- solid-state asymmetric supercapacitors with enhanced performance. J. Mater. Chem. A 5: 10227-10235. DOI: 10.1039/C7TA02558K

Wang X, Hu J, Liu W, Wang G, An J, Lian J (2015) Ni–Zn binary system hydroxide, oxide and sulfide materials: synthesis and high supercapacitor performance. J. Mater. Chem. A 3 : 23333–23344. DOI: 10.1039/C5TA07169K

Xie Q, Ma Y, Zeng D, Wang L, Yue G, Peng D.L (2015) Facile fabrication of various zinc-nickel citrate microspheres and their transformation to ZnO-NiO hybrid microspheres with excellent lithium storage properties. Sci. Rep. 5 : 8351–8359. DOI: 10.1038/srep08351

Zheng S, Xue H, Pang H (2017) Supercapacitors based on metal coordination materials, Coord. Chem. Rev. https://doi.org/10.1016/j.ccr.2017.07.002

Zhong Z, Li Q, Zhang Y, Zhong H, Cheng M, Zhang Y (2005) Synthesis of nanocrystalline Ni-Zn ferrite powders by refluxing method. Powder Technol. 155 : 193–195. doi:10.1016/j.powtec.2005.05.060

Figure. 1: XRD patterns of obtained Ni-Zn (1:1 **(a)** and 1:2 **(b)**) bi-phase nanohybridsusing urea based hydrothermal process with different experimental parameters.

Figure. 2: FTIR spectra of obtained Ni-Zn bi-phase nanohybrids using urea based hydrothermal method with different experimental parameters.

Figure. 3: Raman spectroscopy spectra of Ni-Zn (1:1 and 1:2) based heterostructure hydroxides synthesized by hydrothermal method at two different growth temperature.

Figure. 4: FESEM micrographs of obtained micro-nanostructures based of Ni-Zn bi-phase nanohybrids at two different growth temperatures and Ni:Zn precursors ratio: 1:1 (**a.a'.** 6h-120°C, **b.b'.** 6h-180°C), 1:2 (**c.c'.** 6h-120°C, **d.d'.** 6h-180°C).

Figure. 5: N_2 adsorption–desorption isotherms (**up**) and the corresponding pore size distribution (**down**) of the synthesized Ni-Zn based micro-nanostructures using hydrothermal method at two different growth temperature and Ni/Zn precursors ratio.

Figure. 6: XPS survey scan spectra (**A**) and percentage composition depending to the synthesis condition (**B** and **C**).

Figure. 7: XPS spectra of these Ni-Zn bi-hydroxides micro-nanosystems in the Ni_{2p}, Zn_{2p}, C_{1s}, O_{1s} energy regions at different conditions: (**a: 6h/120°C** and **b: 6h/180°C**).

Table. 1: Physico-chemical characteristicsof the synthesized bi-hydroxide based 3D micro-nanohybrids.

Figure 1A
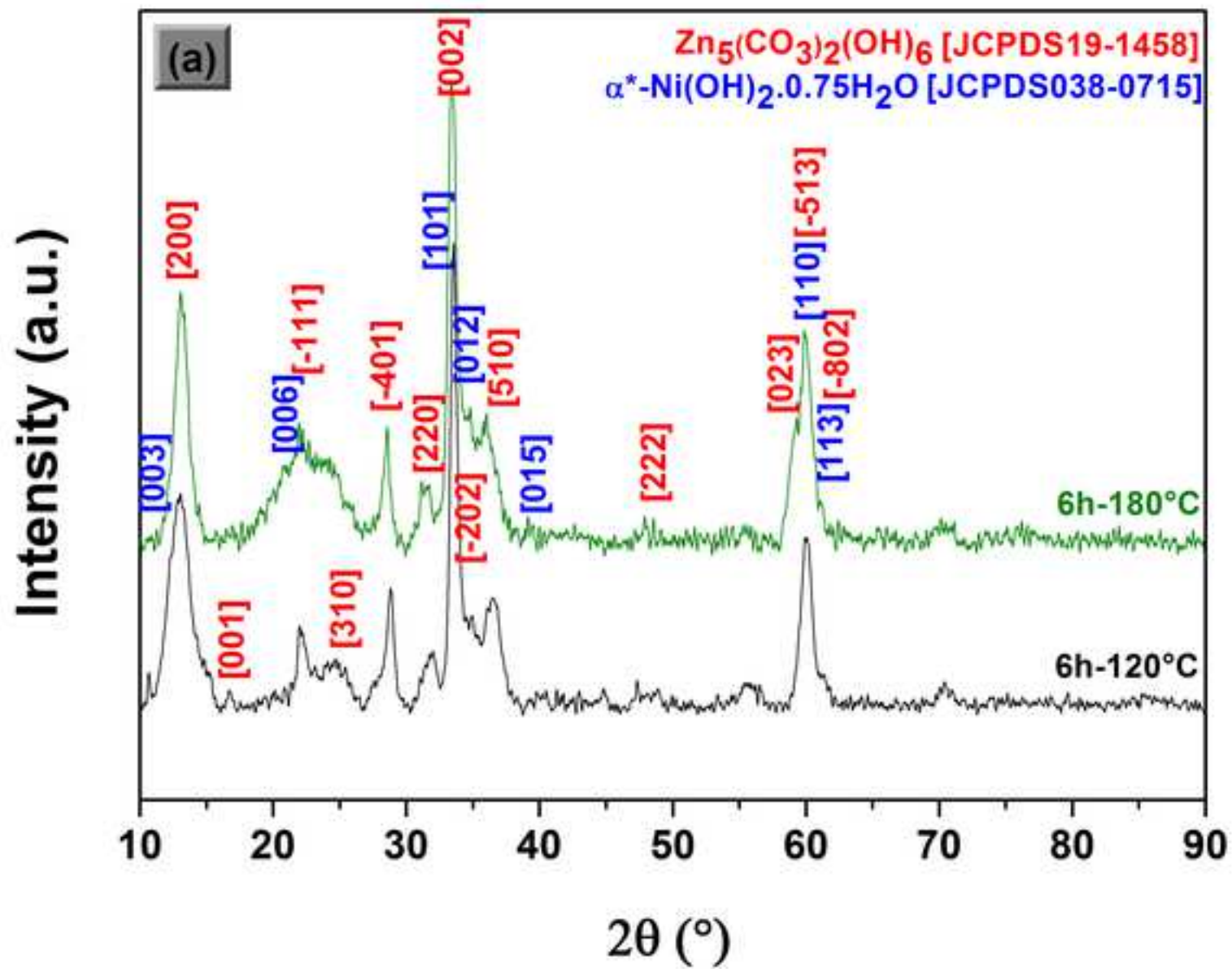
Figure 1B
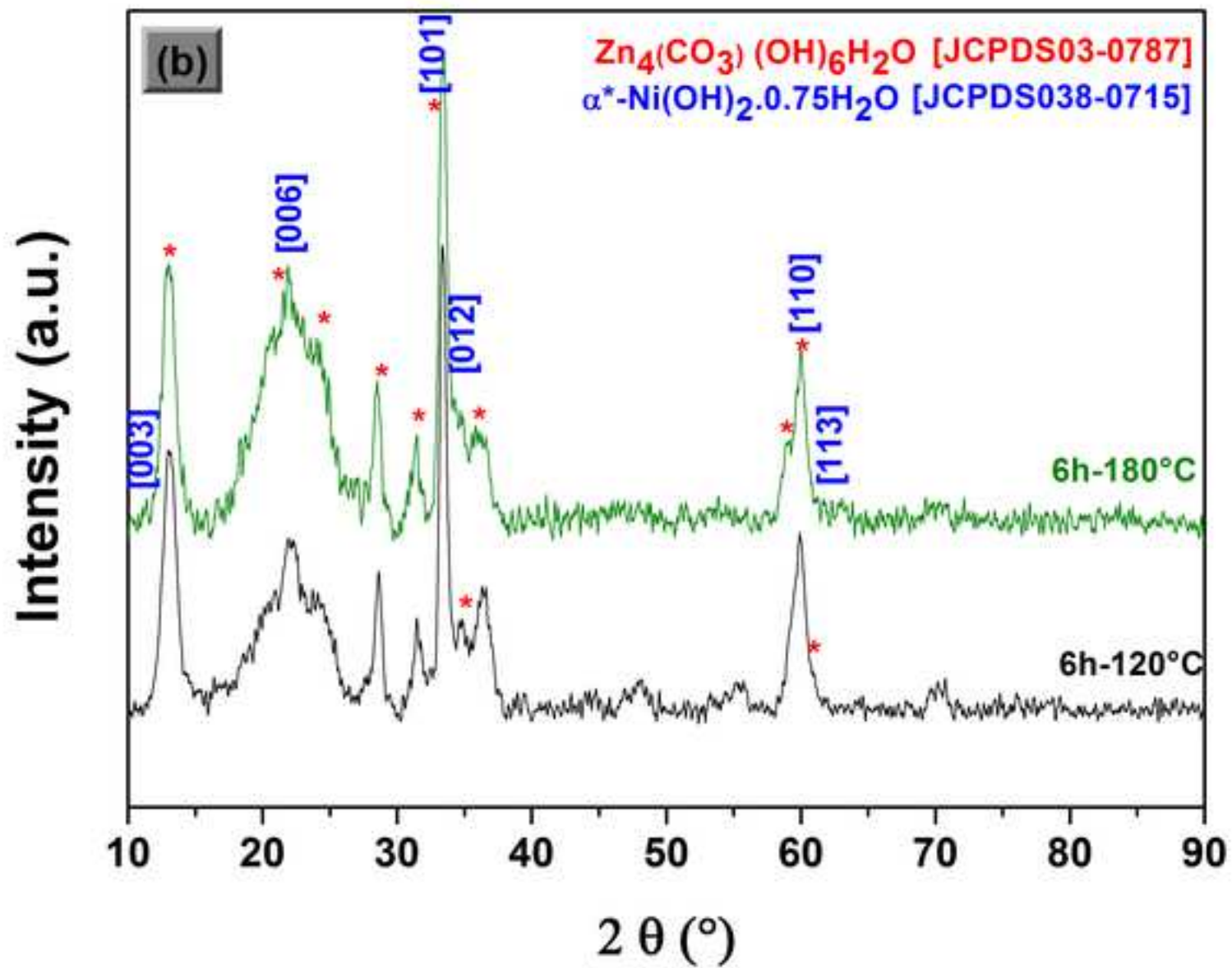
Figure 2
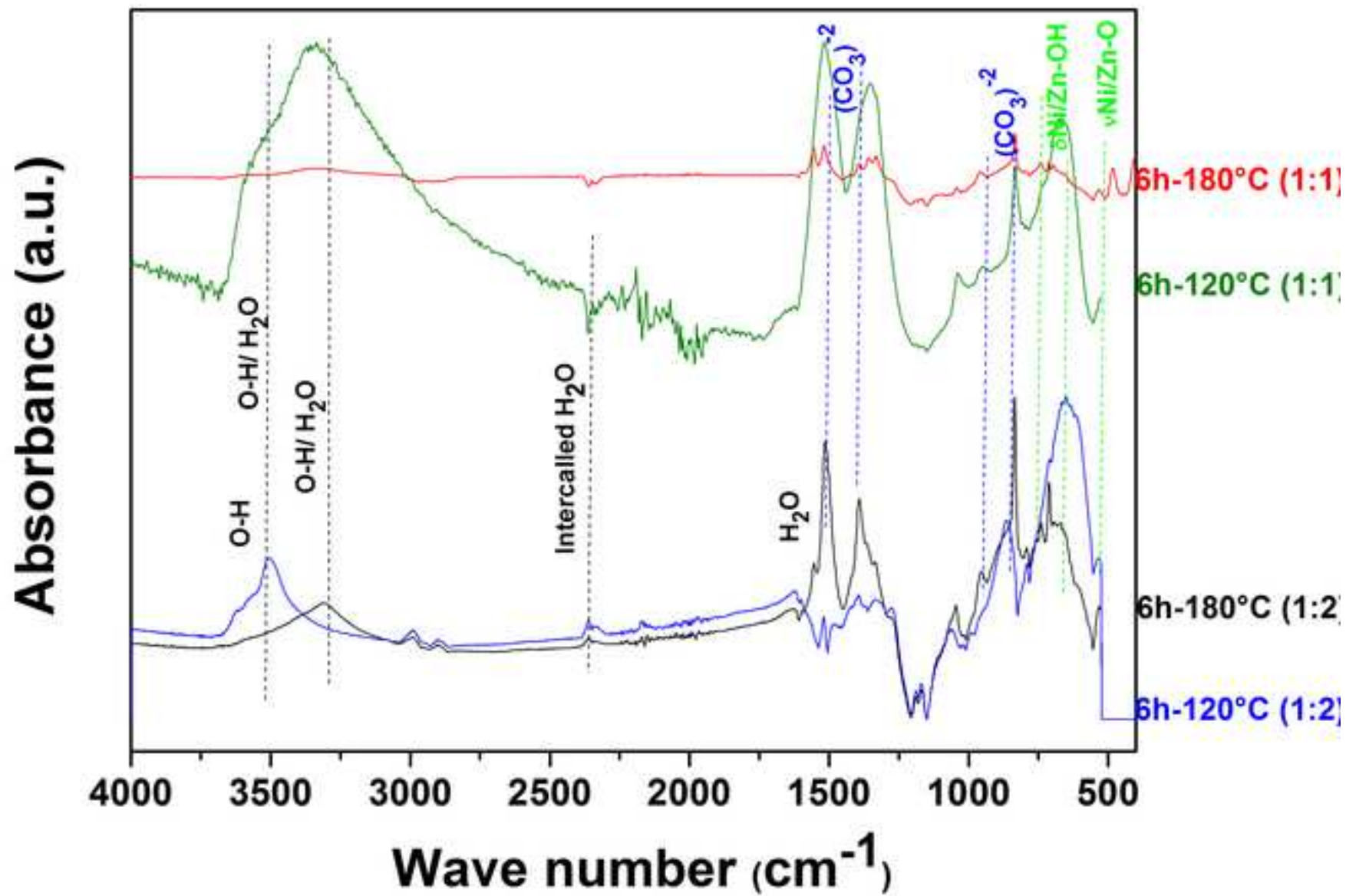
Figure 3
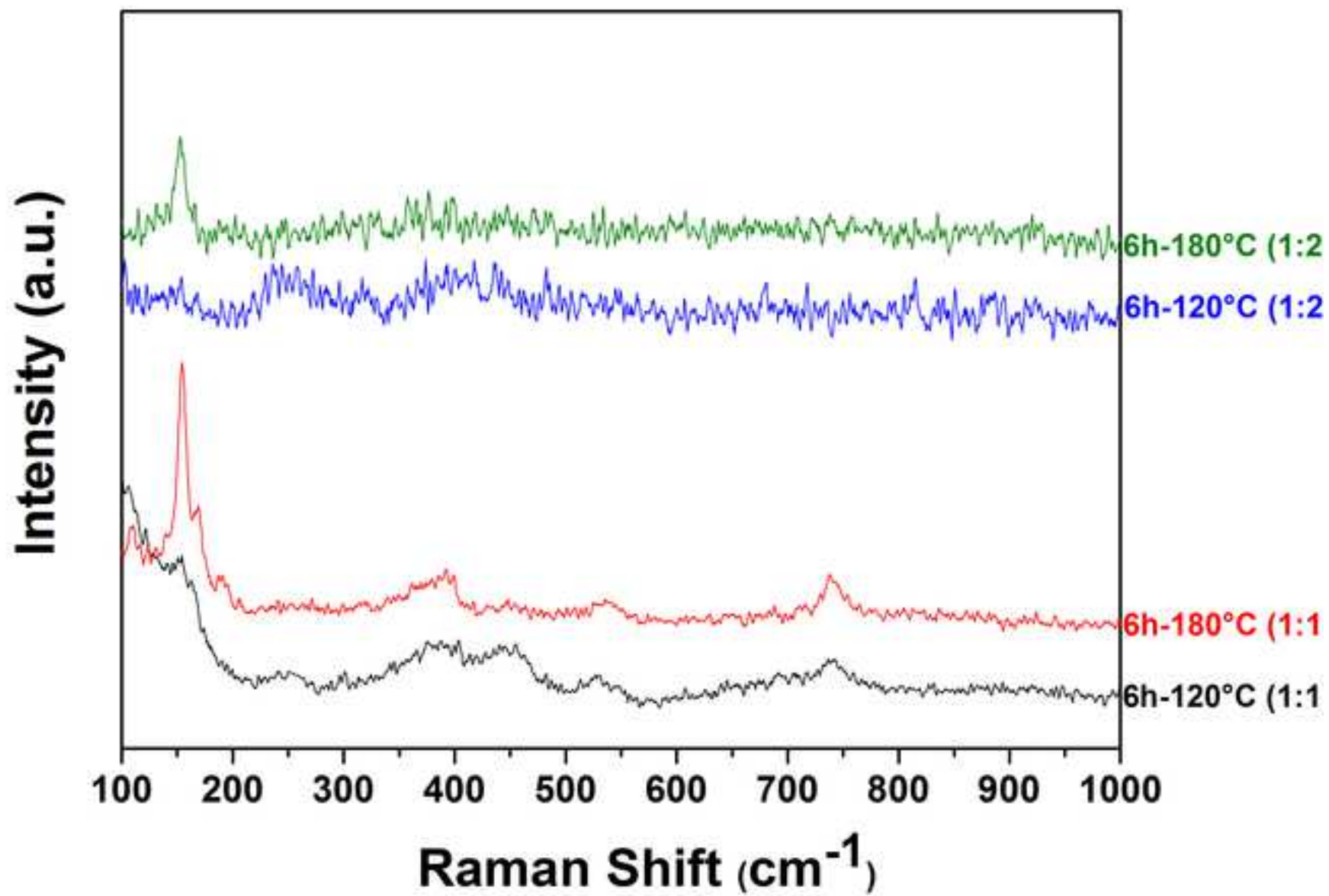
Figure 4
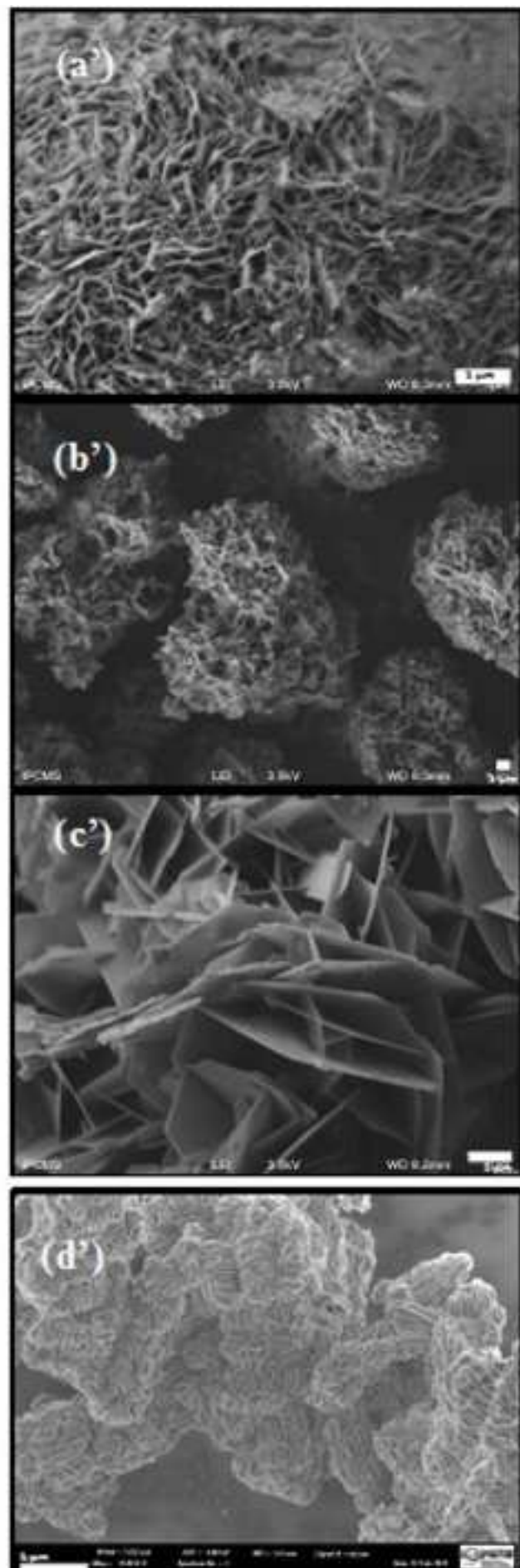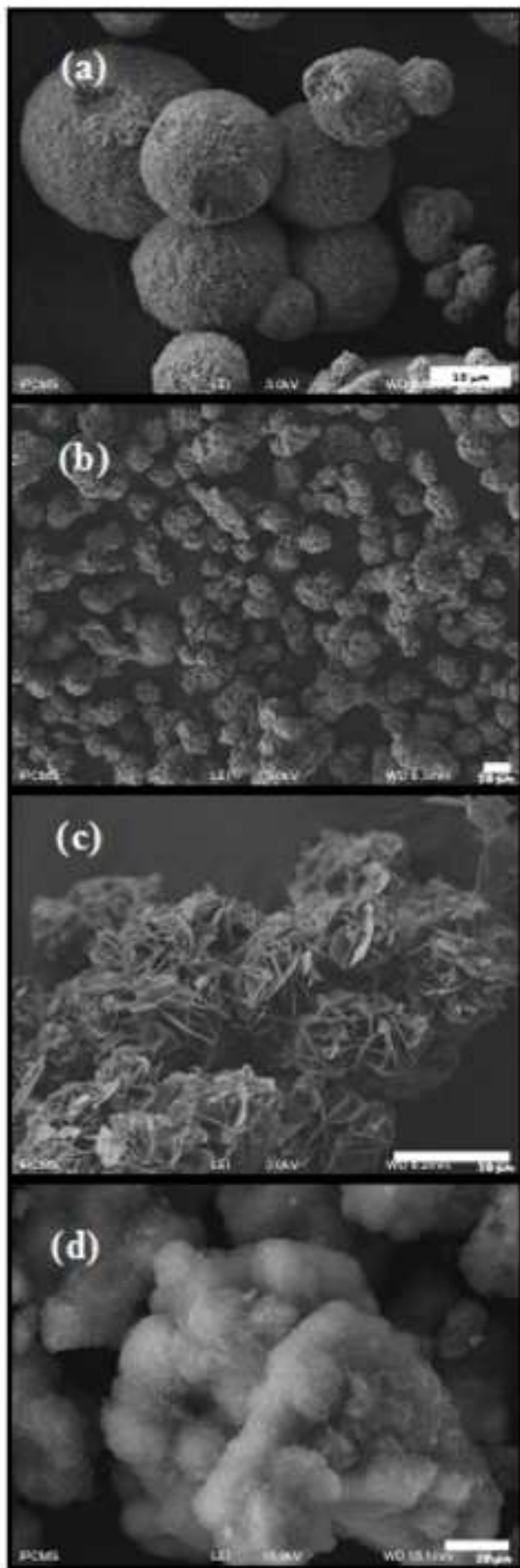
Figure 5A

Figure 5B
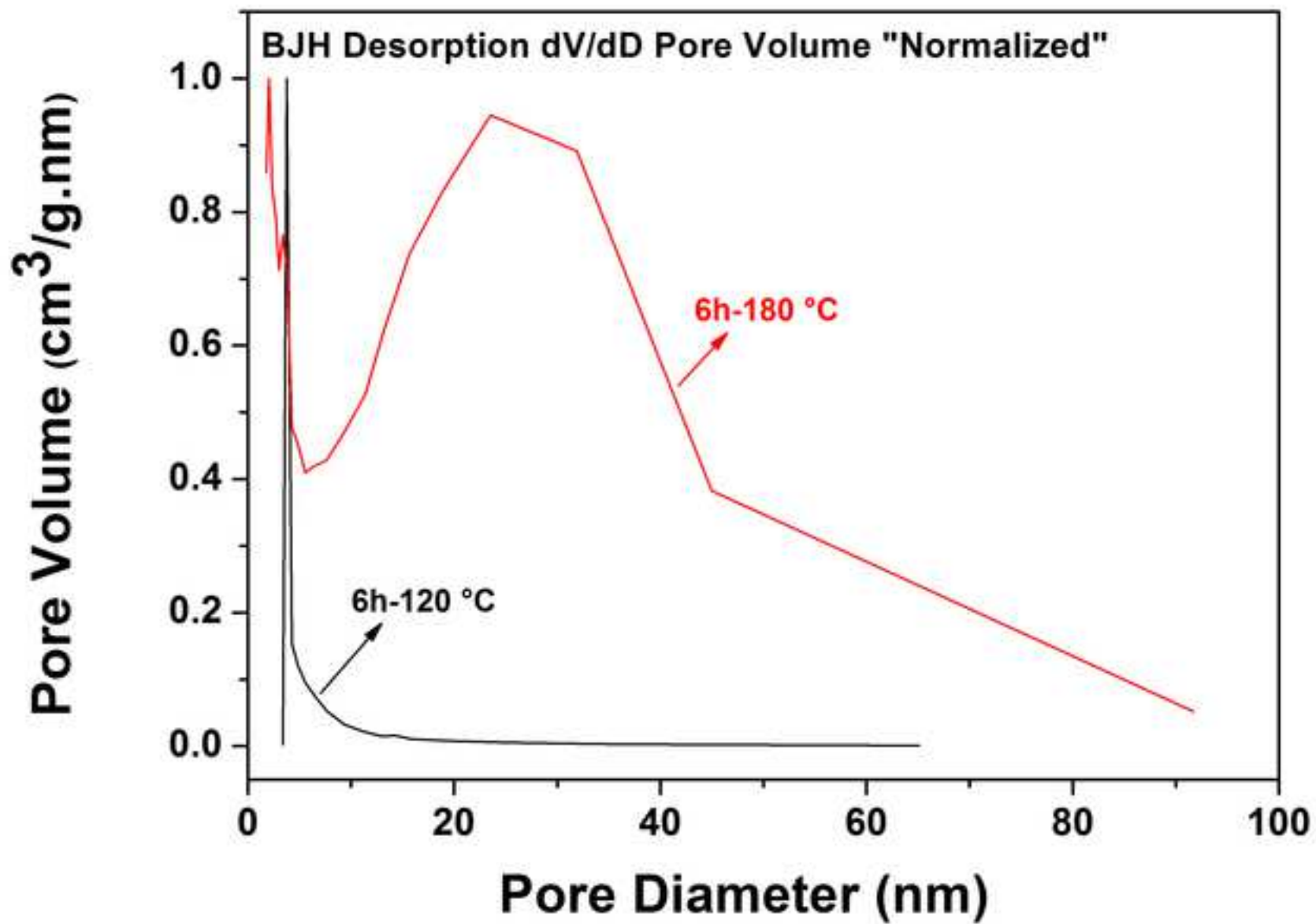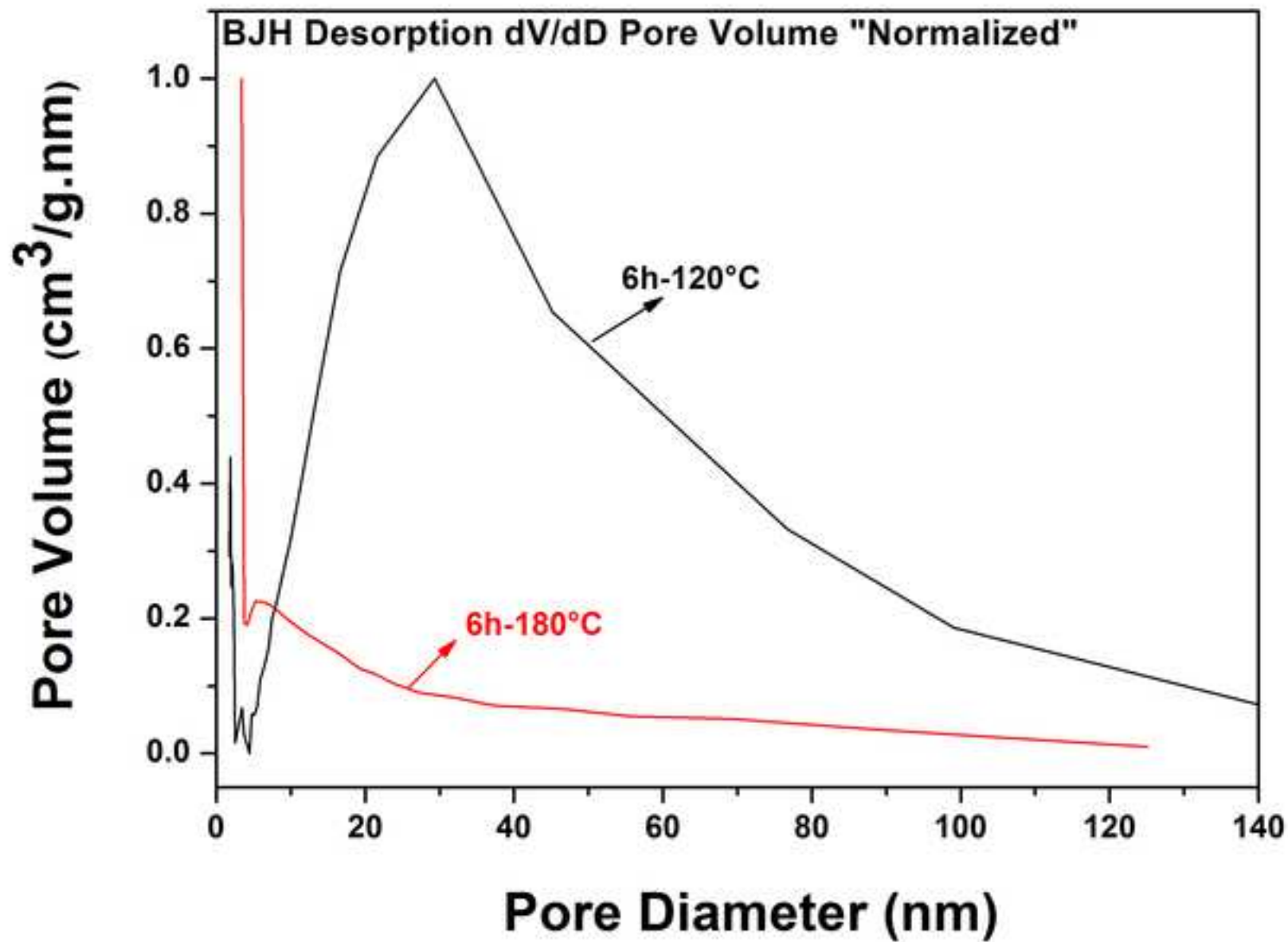
Figure 5C
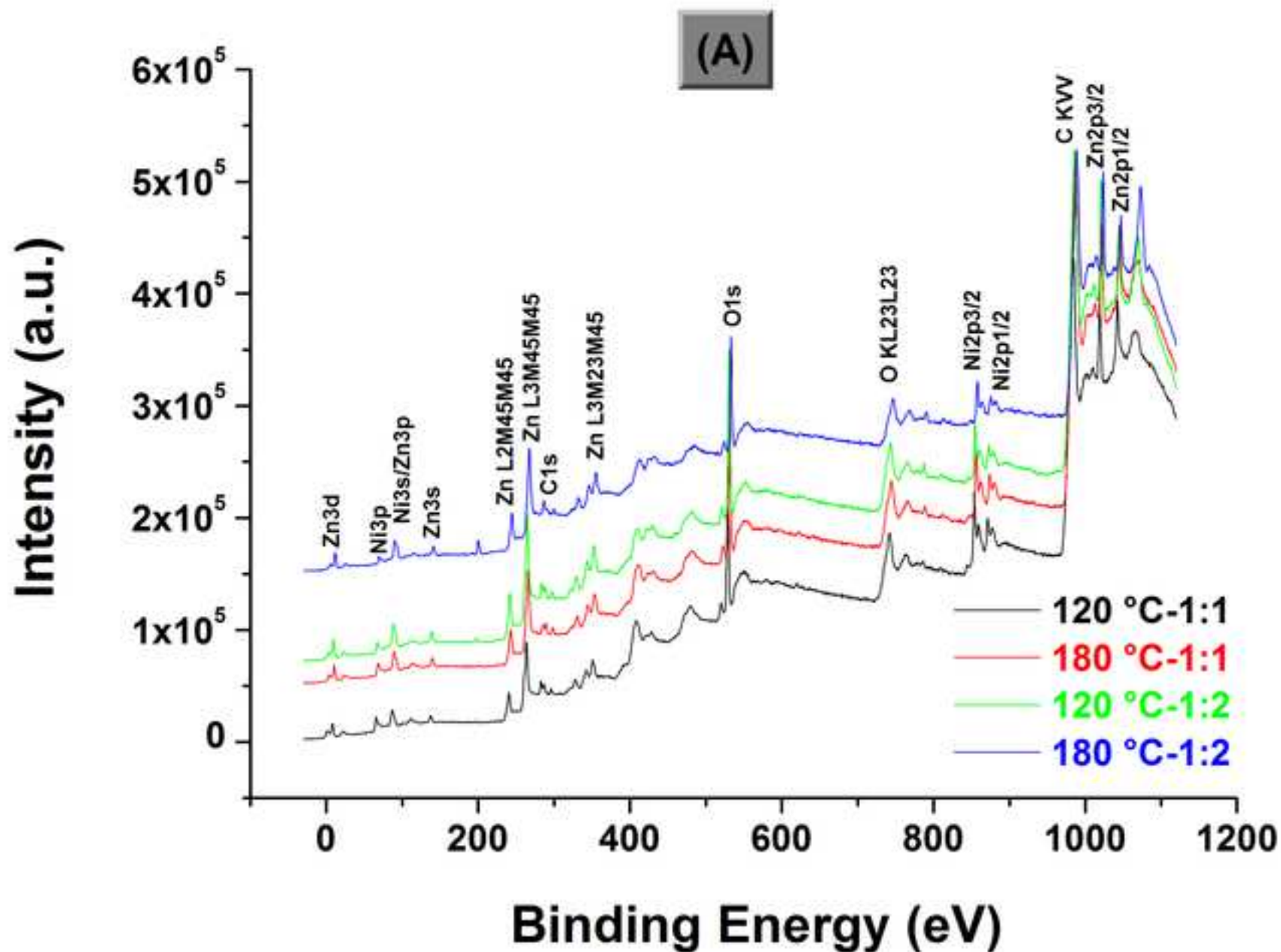

BJH Desorption dV/dD Pore Volume "Normalized"

6h-180 °C
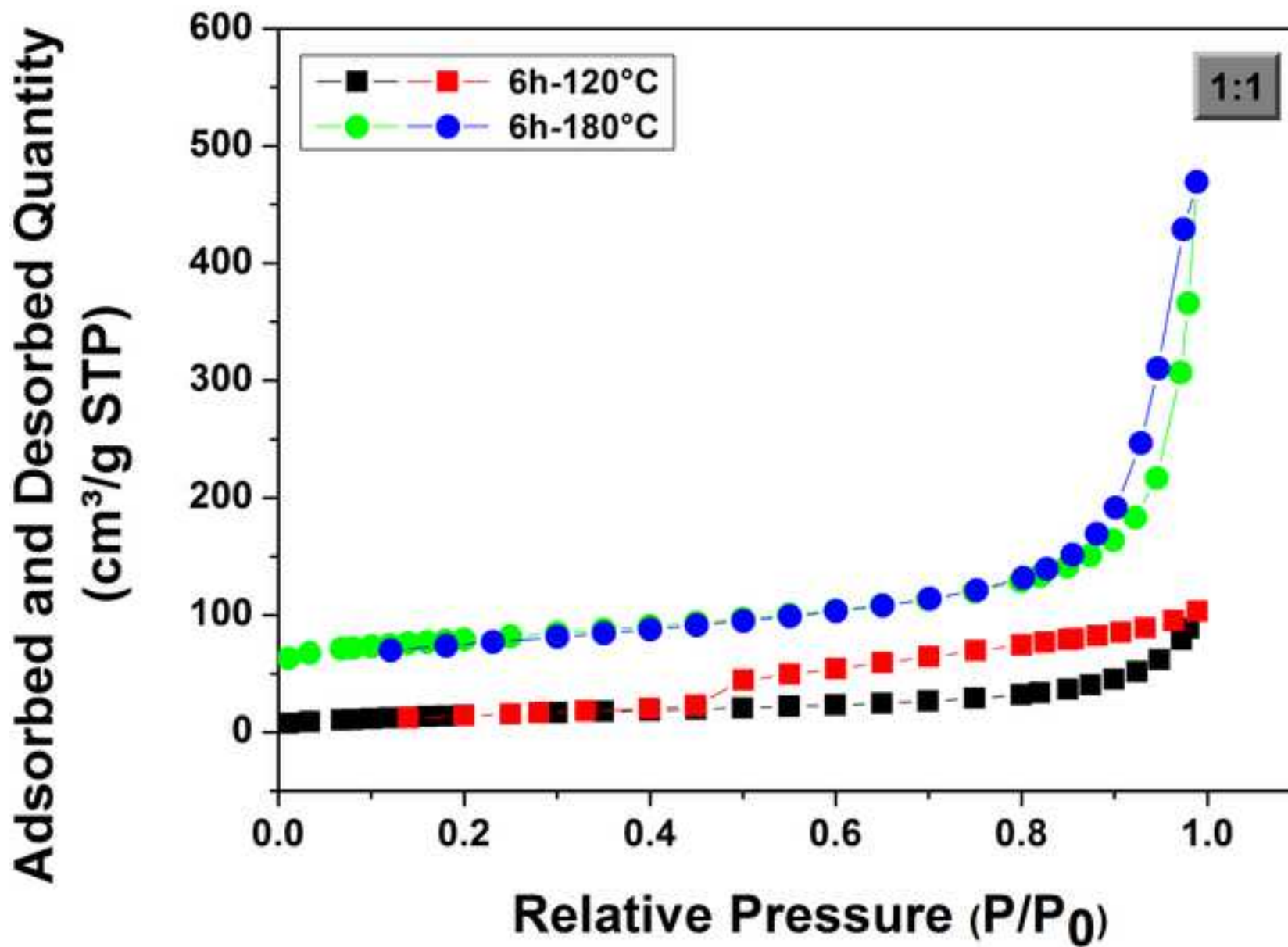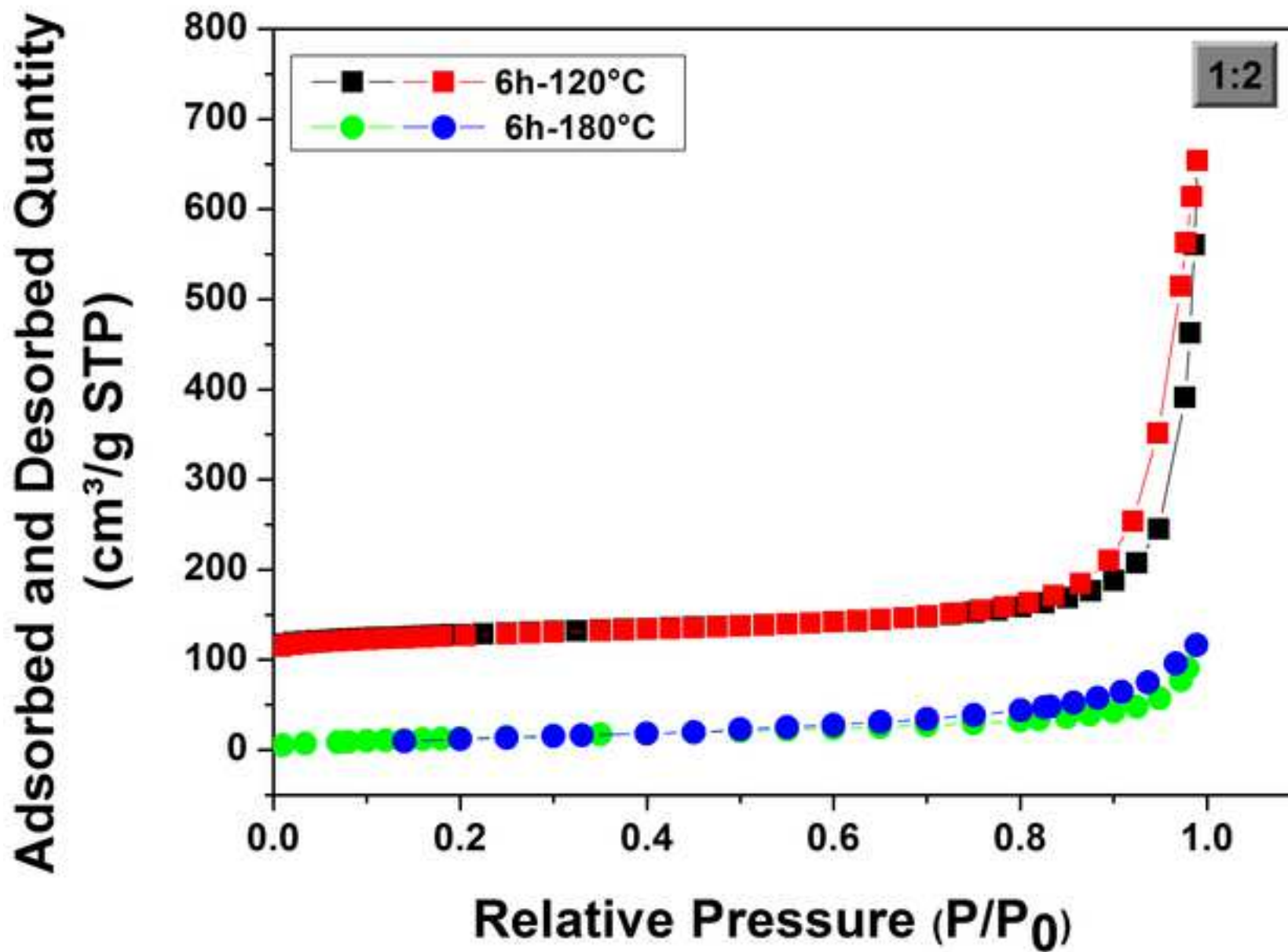
6h-120 °C

Figure 5D

Figure 6A

Figure 6B

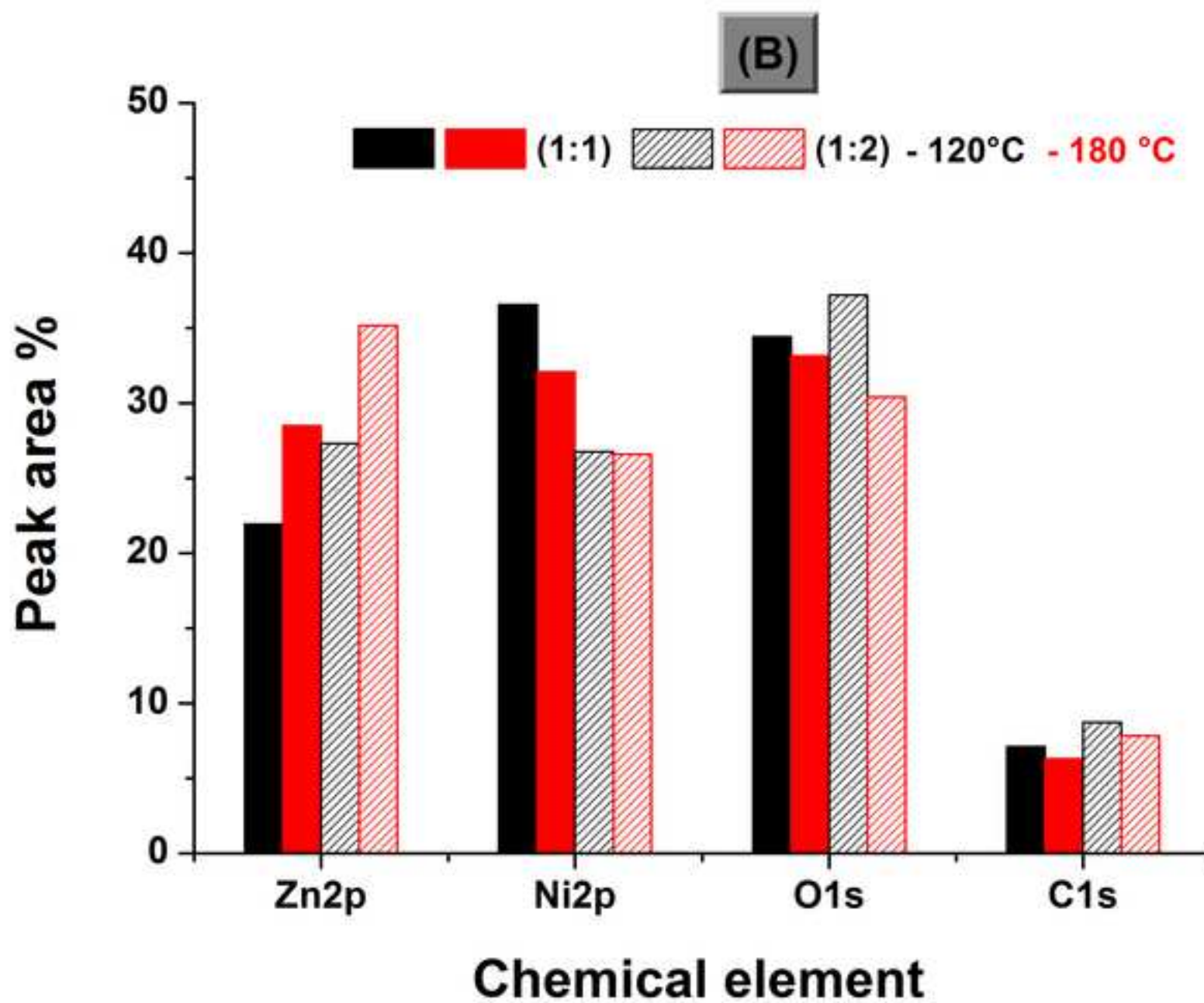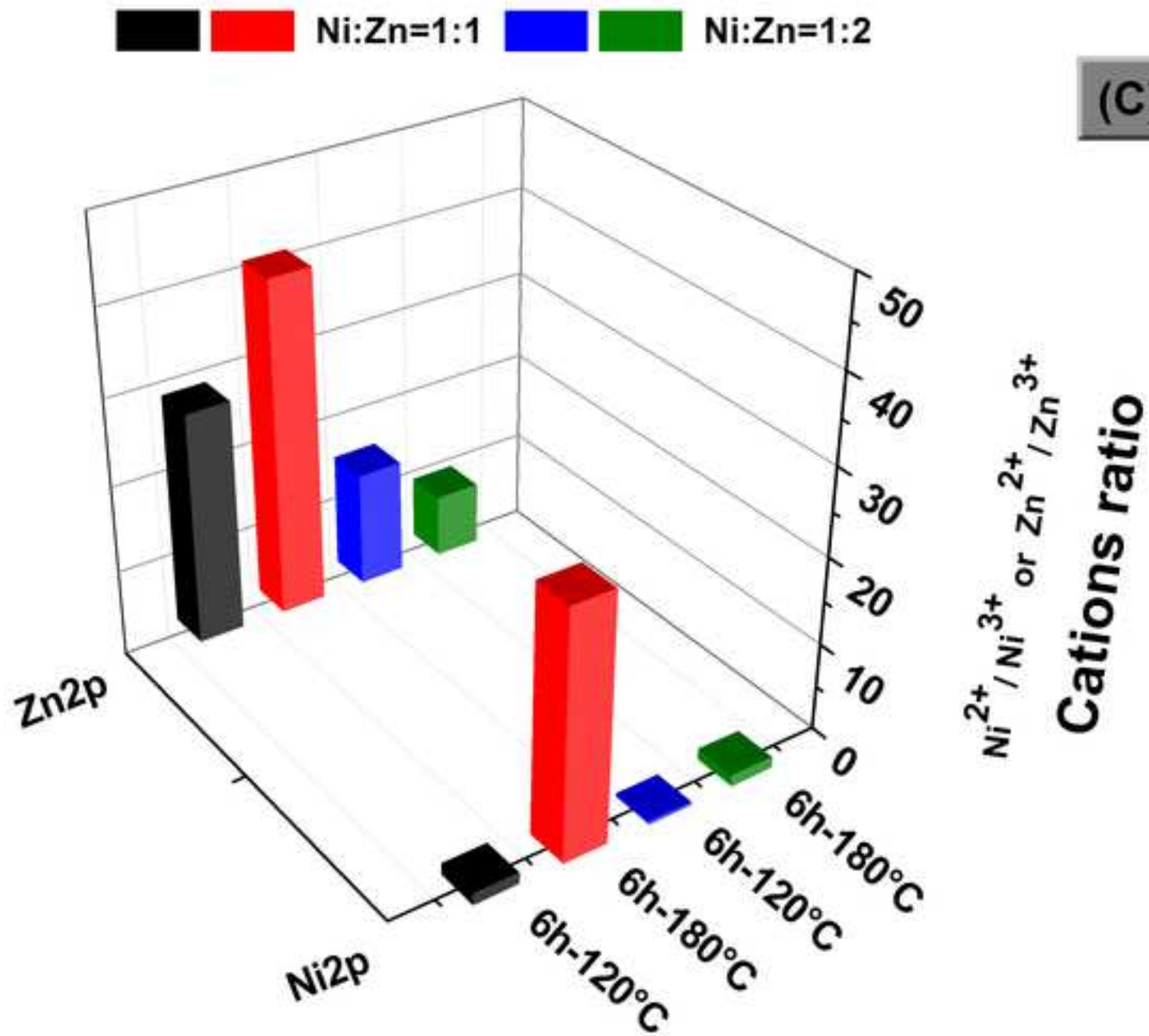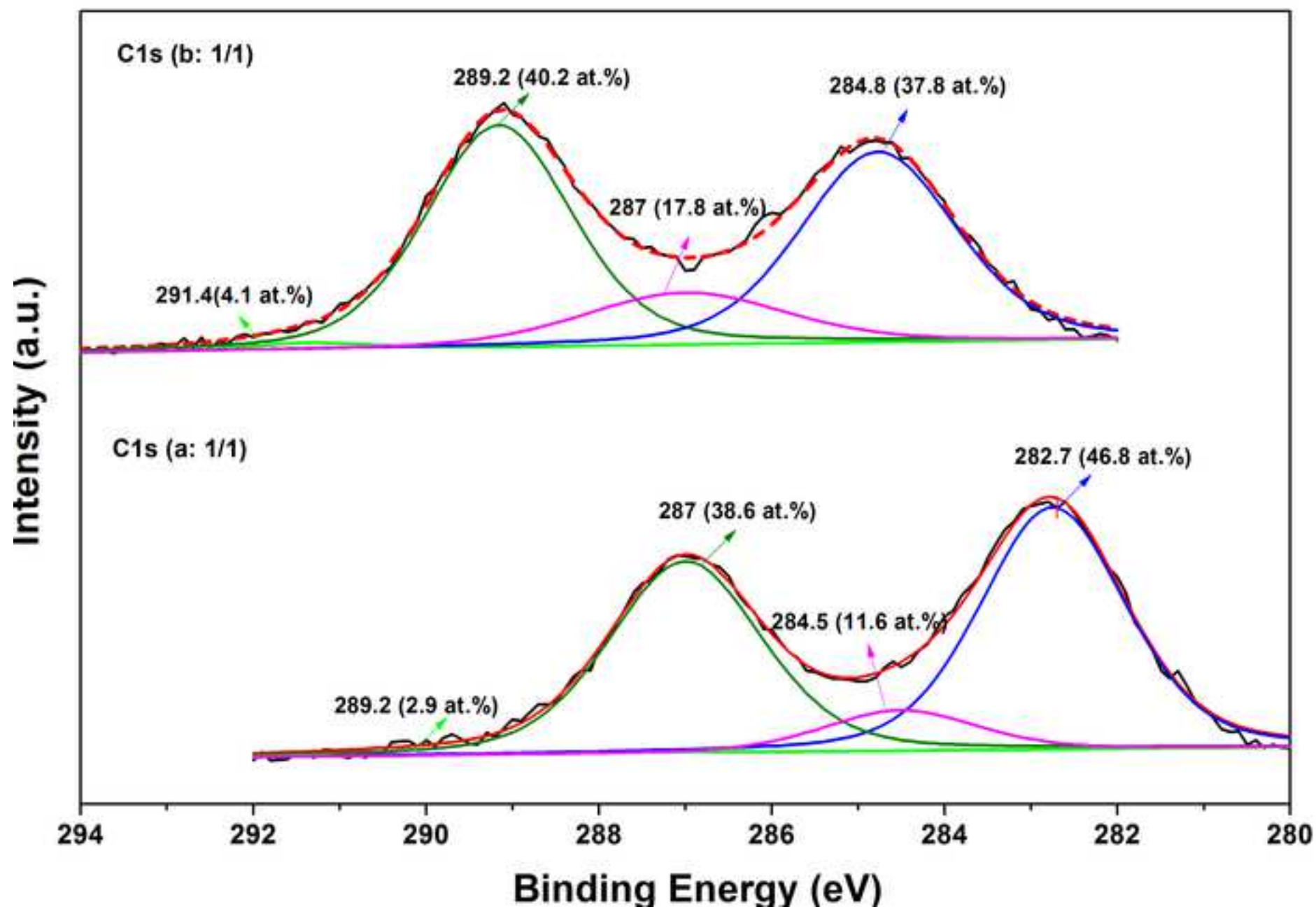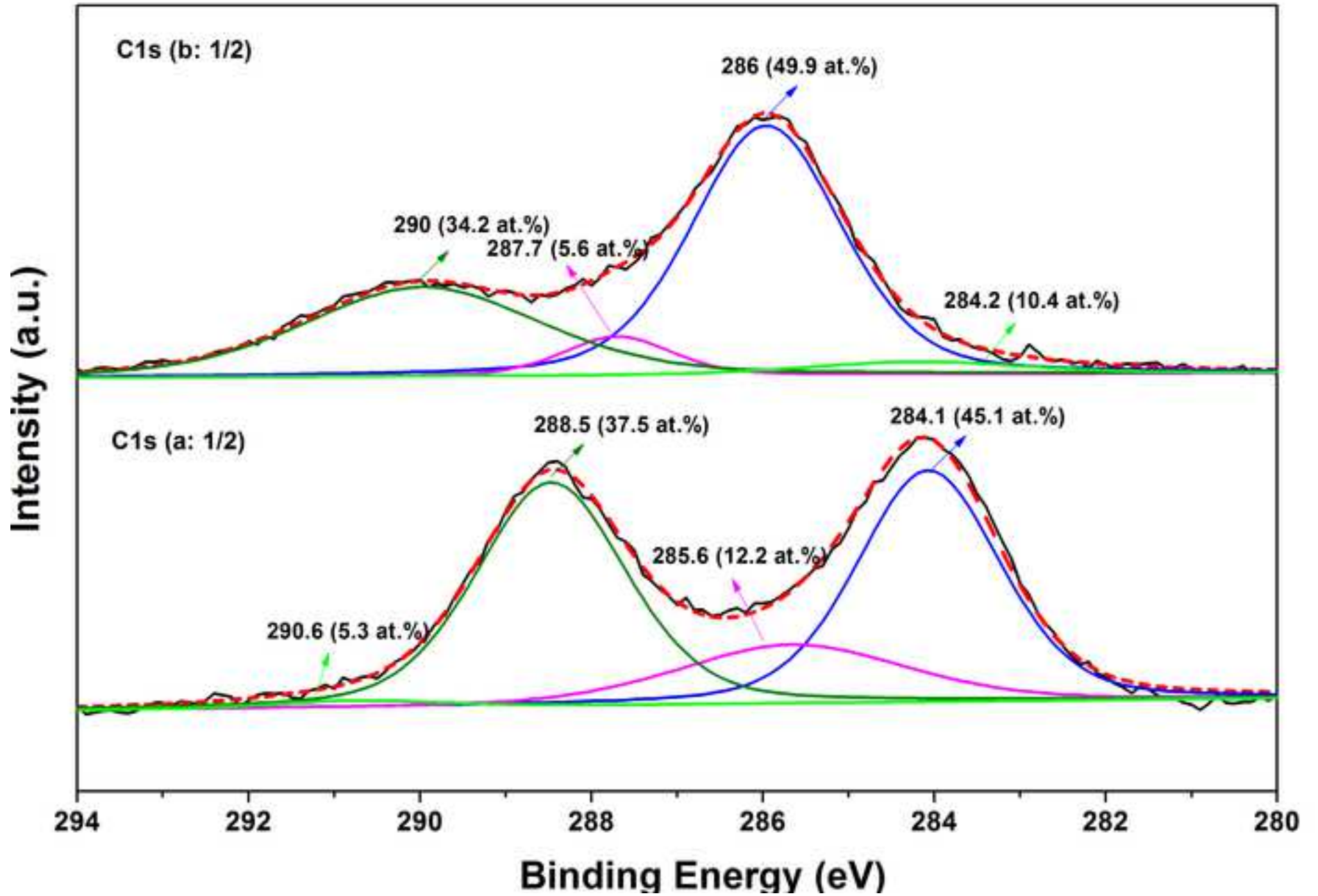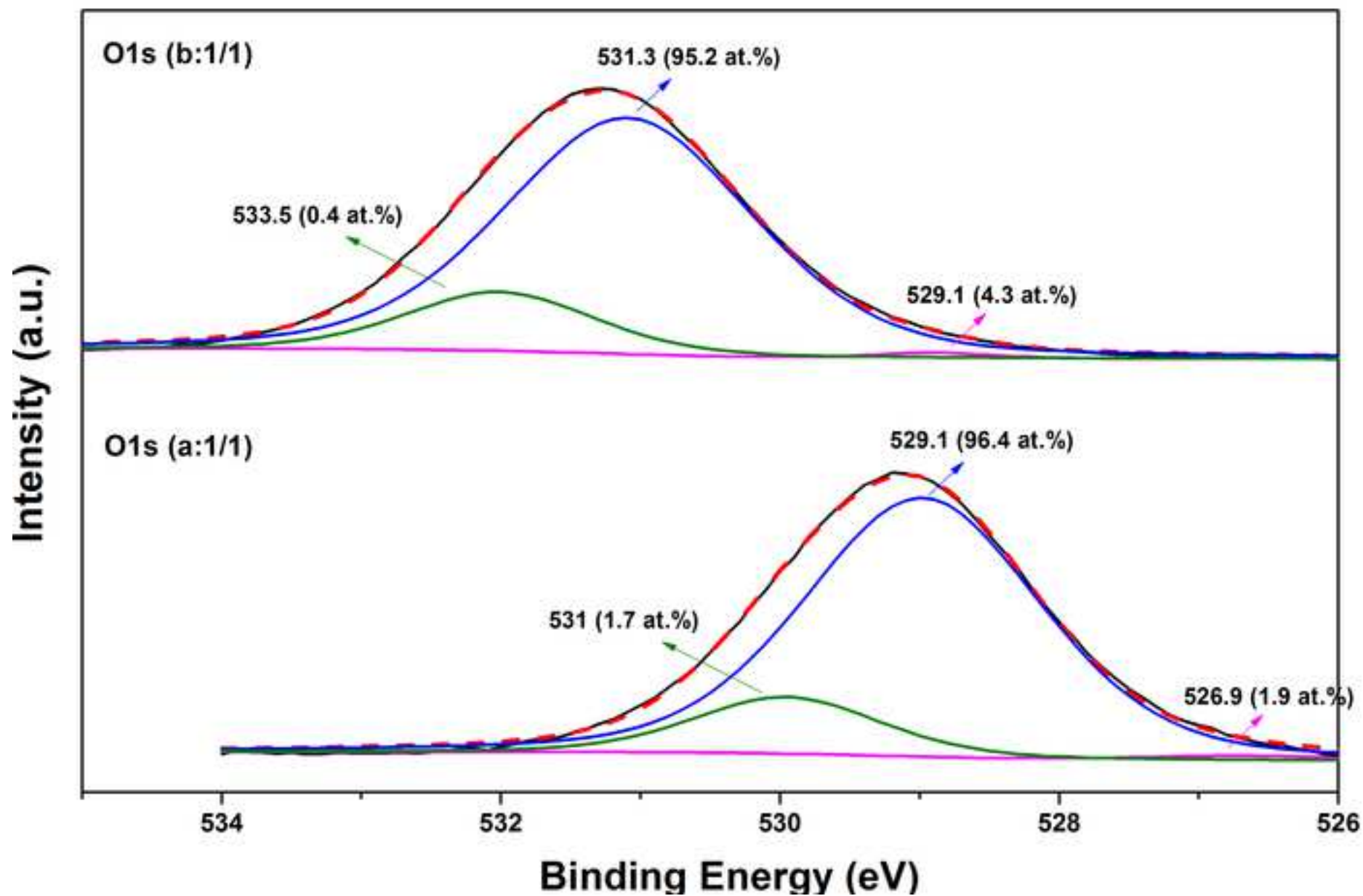Figure 6C

Figure 7a

Figure 7b

Figure 7c

Figure 7d
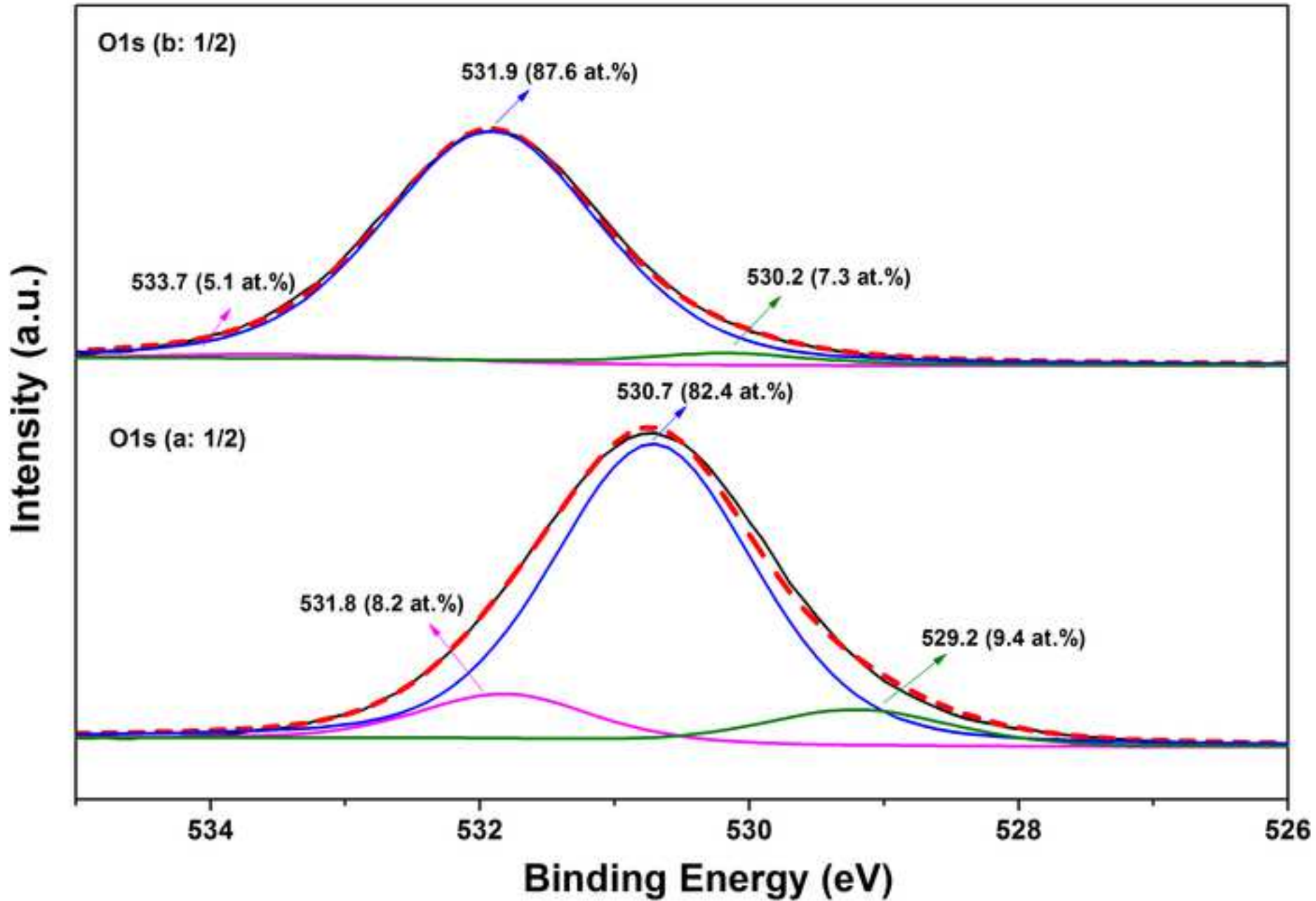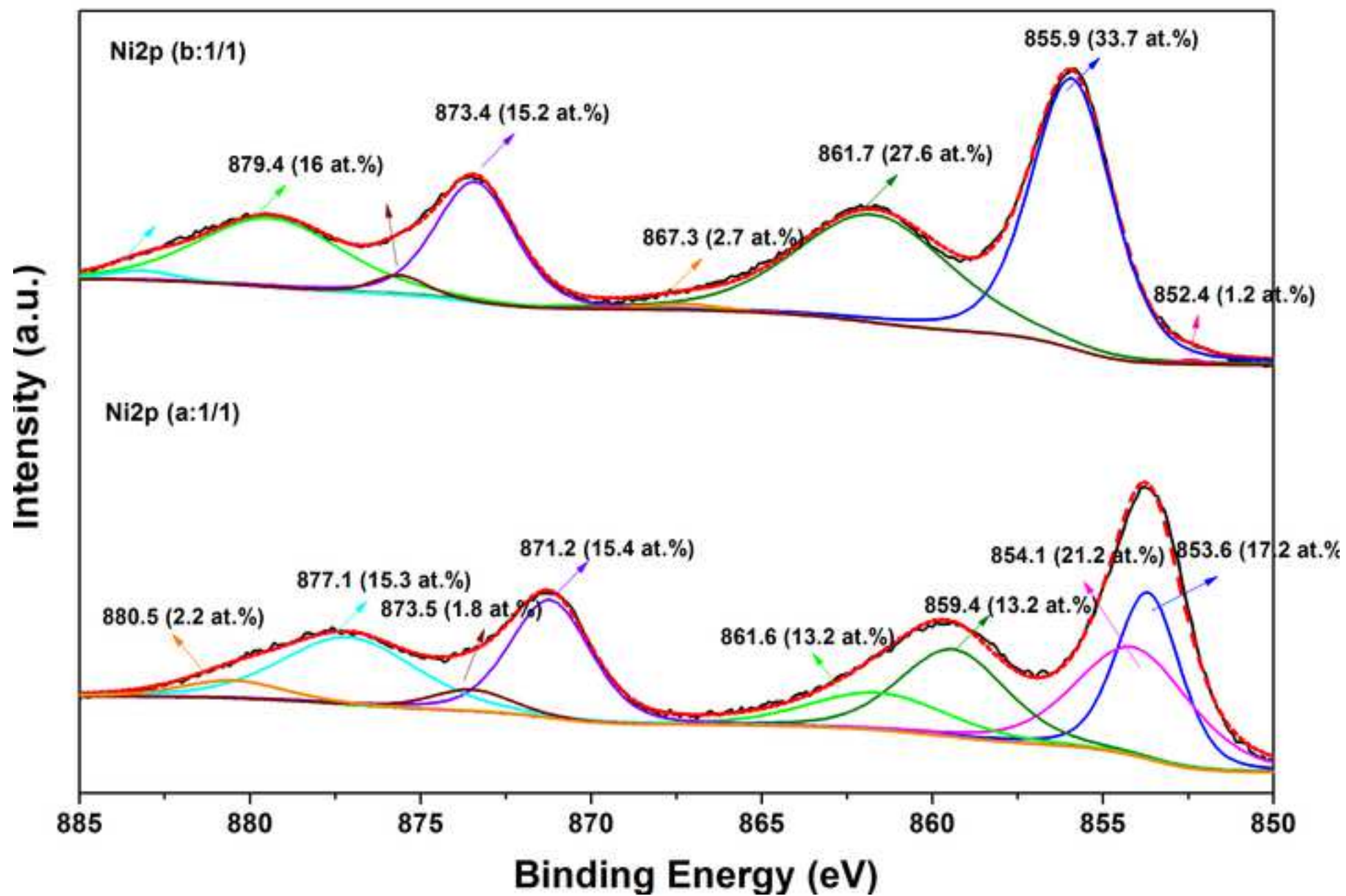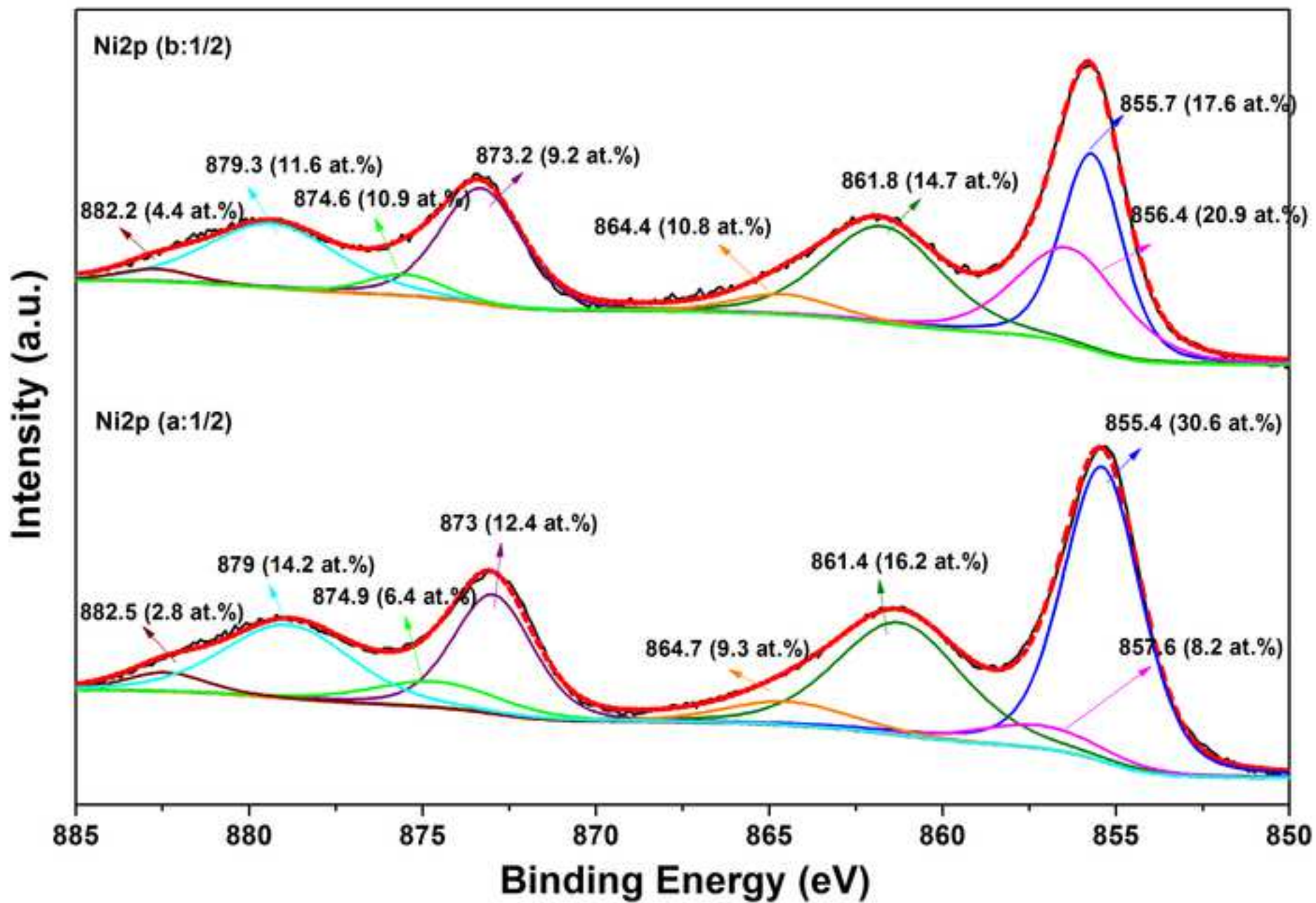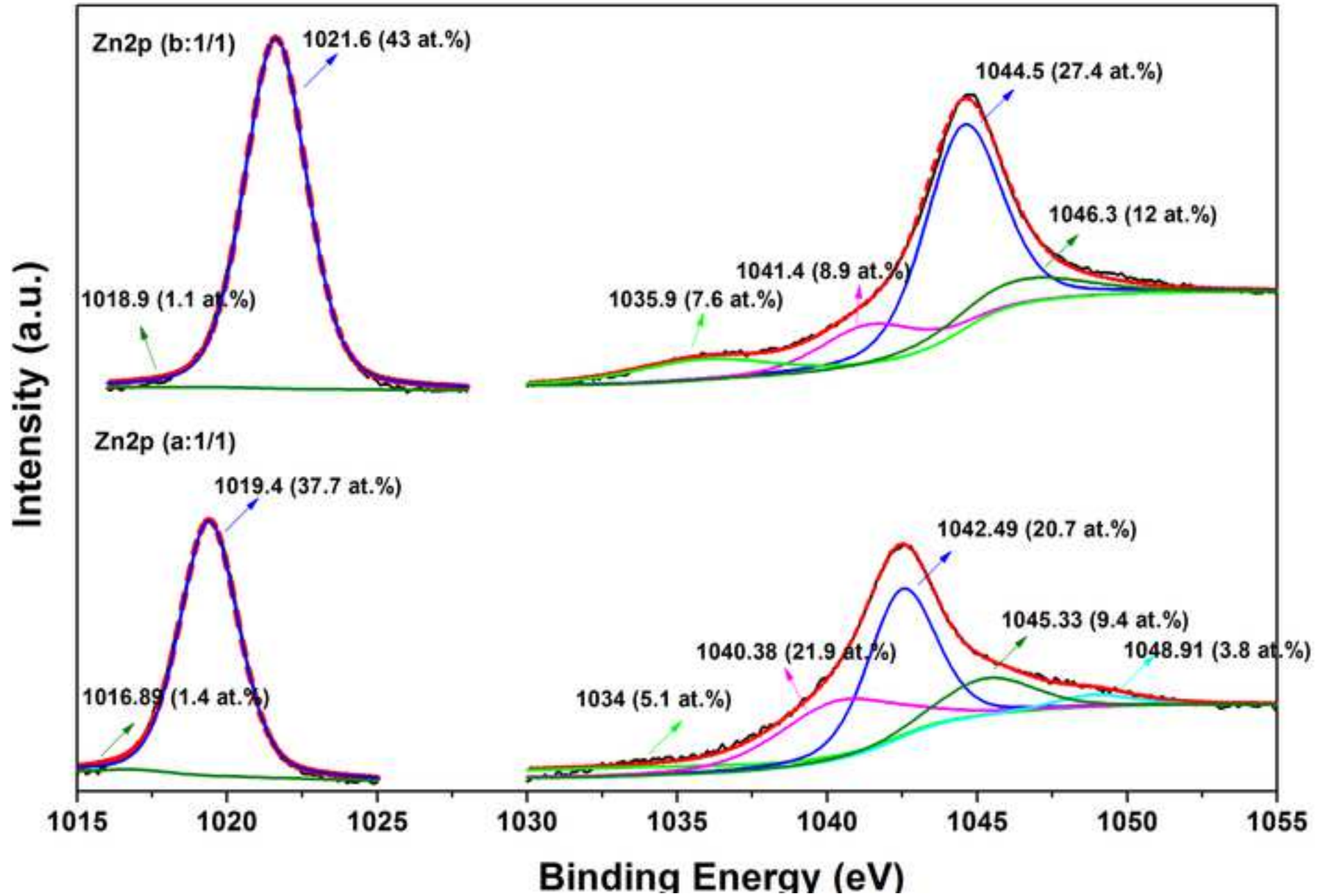
Figure 7e

Figure 7f

Figure 7h

Zn2p (b:1/2)
- 1021.5 (44 at.%)
- 1020.4 (6.2 at.%)
- 1023.7 (1.7 at.%)
- 1044.5 (25.4 at.%)
- 1046.5 (2.5 at.%)
- 1042.3 (12.1 at.%)
- 1035.6 (8.2 at.%)

Zn2p (a:1/1)
- 1021.1 (45 at.%)
- 1019.5 (3.4 at.%)
- 1023.1 (2.9 at.%)
- 1044.2 (24.1 at.%)
- 1042.3 (9.5 at.%)
- 1047.8 (9.8 at.%)
- 1035.4 (4.7 at.%)

Intensity (a.u.)

Binding Energy (eV)